NON-INVASIVE IMAGING OF LYMPHATIC REMODELING IN RESPONSE TO INJURY THROUGH PHOTODYNAMIC THERAPY

A Thesis
Presented to
The Academic Faculty

By

Yanina Kuzminich

In Partial Fulfillment
of the Requirements for the Degree
Master of Science in Bioengineering

Georgia Institute of Technology

December 2020

NON-INVASIVE IMAGING OF LYMPHATIC REMODELING IN RESPONSE TO INJURY THROUGH PHOTODYNAMIC THERAPY

Approved by:

Dr. J. Brandon Dixon, Advisor
The George W.Woodruff School of Mechanical Engineering
Georgia Institute of Technology

Dr. Erin M. Buckley
Wallace H.Coulter Department of Biomedical Engineering
Georgia Institute of Technology

Dr. Rudolph L. Gleason
The George W.Woodruff School of Mechanical Engineering
Georgia Institute of Technology

Date Approved: August 7, 2020

To the memory of my beloved grandmother Galina Kuzminich

ACKNOWLEDGEMENTS

Firstly, I would like to thank my advisor, Dr. J. Brandon Dixon, for his professional guidance, patience, and support that were essential for this research project. His knowledge, critiques, and insight helped me to broaden my scientific perspectives.

I would like to express my sincere gratitude to Dr. Ruediger Naumann-Etienne for funding my education and making my attendance of Georgia Tech possible. Thanks to his generosity I was able to fulfill my dream of studying Bioengineering at one of the top universities in the USA.

Additionally, I would like to thank my lab mates and friends, especially Ada Del Cid, Oksana Iushchak, Heorghi Kolas, Stephen Robinson, Valeryia Shlapak, and Jakub Srna for their incredible support regardless of the distance between us.

Also I wish to thank Oksana and Gregory Berzonsky, for openly and generously sharing their warmth and kindness with me in this unprecedented time.

Finally, I would like to thank my mother, Alena Kuzminich, for her love and encouragement to pursue my passions and all my family for their endless support throughout those years.

TABLE OF CONTENTS

LIST OF TABLES

LIST OF FIGURES

LIST OF ABBREVIATIONS

AMD Age-related macular degeneration

APC Antigen-presenting cells

CT Computed tomography

DC Dendritic cell

DiH_2O Distilled water

DMSO Dimethyl sulfoxide

DOB Date of birth

EMCCD Electron-multiplying charge-coupled device

FAK Focal adhesion kinase

FWHM Full width at half maximum

HDL High-density lipoprotein

ID Intradermal

IFN-γ Interferon gamma

LDL Low-density lipoprotein

LDLR Low-density lipoprotein receptors

LEC Lymphatic endothelial cell

LMC Lymphatic muscle cell

MRI Magnetic resonance imaging

MRL Magnetic resonance lymphangiography

NIR Near-infrared imaging

PAT Prenodal adipose tissue

PDT Photodynamic therapy

PEG Polyethylene glycol

PET Positron emission tomography

ROI Region of interest

ROS Reactive oxygen species

SD Standard deviation

SEM Standard error of the mean

SPECT Single-photon emission computed tomography

TNF-α Tumor necrosis factor-α

VEGFR3 Vascular endothelial growth factor receptor-3

VP Verteporfin

SUMMARY

The lymphatic system is an essential but often understudied in comparison with its cardiovascular counterpart. Such disparity could often be explained by the lack or complexity of the existing imaging and analysis techniques available for the quantification of lymphatics compared to the ones available for the blood vasculature. An additional challenge is the absence of representative *in vivo* models that efficiently replicate the lymphatic dysfunction observed in humans. Those factors motivate the continuous investigation of novel models for lymphatic diseases and ways to evaluate the overall function of the lymphatic system. Recently, it has been shown that verteporfin, a photosensitive drug widely used for photodynamic therapy (PDT) to ablate the blood vessels, provides a similar effect on lymphatic vessels. Here, we seek to administer verteporfin and perform PDT of collecting lymphatics in the mouse tail, which is a commonly used location for the study of lymphatic disorders and examine lymphatic remodeling, contractility, and transport in response to the procedure. To quantify the induced changes, the lymphatic function was evaluated using a near-infrared (NIR) imaging system. Additional image processing has been introduced to access the NIR tracer distribution following the lymphatic injury caused by the verteporfin administration. As a result, we are able to increase lymphatic permeability noninvasively at the targeted area. This technique has the potential to be a stand-alone procedure to investigate the lymphatic response to a localized leakage and reactive oxygen species (ROS) and serve as an improvement to existing *in vivo* models of lymphatic disorders.

CHAPTER 1
INTRODUCTION

The lymphatic system is a network of lymphatic vessels and lymphoid organs, distributed around the body, that plays a major role in lipid transport [1], fluid homeostasis [2] and immune cell trafficking [3]. The lymphatics unidirectionally transport lymph, a fluid containing proteins, from interstitial space back to the blood circulation [4]. While in the cardio-vascular system the heart is the central pump for blood transport, propagation of the lymph is not driven by a single centralized pump. Instead, a combination of external tissue pressures and an internal pump mechanism driven by contractions of lymphatic muscle cells, are responsible for lymph movement. The lymphatic system transfers 4-8 liters of fluid back into the blood stream daily through the collecting ducts [5] and it is estimated that as much as 12 liters of lymph per day is returned in total to the circulation when one also considers fluid absorption into the venous circulation at regional lymph nodes. The whole system can be considered as fluid storage of filtered plasma [2].

1.1 Lymphatic physiology

The lymphatic system can be divided into several units: initial lymphatics, collecting lymphatics, and lymph nodes[4]. Initial lymphatics are blind-ended vessels or plexus of vessels in peripheral tissues that allow for free diffusion of solutes within them. This is also the site of lymph formation, where fluid enters the lymphatics. Initial lymphatics, or capillaries, are composed of a monolayer of lymphatic endothelial cells (LECs) with no basement membrane [2]. Anchoring filaments connect the extracellular matrix to the lymphatic endothelial cell cytoskeleton via transmembrane $\alpha 3 \beta 1$ integrin and focal adhesion kinase (FAK) [2, 6, 7]. Anchoring filaments are supporting the attachment of the lymphatic wall to the surrounding tissues [8] and are thought to facilitate fluid entry into the initial vessel

lumen when the surrounding tissue expands.

From initial lymphatics, lymph is drained to pre-collecting and collecting lymphatic vessels (CLVs). Collecting lymphatics organization resembles a binary tree, while the initial lymphatics represent a system of fractals, which cover large areas of the tissue [9]. The pre-collecting lymphatics have one-way valves, but lack lymphatic muscle, and sometimes appear between initial and collecting lymphatics [10]. Meanwhile, collecting vessels are surrounded by lymphatic muscle cells (LMCs) with the lumen of the vessel aligned with LECs, and contain bicuspid valves to prevent backflow [11, 12]. LMCs of the lymphatic vessels are highly contractile, regulating both vessel tone as well as driving the phasic contractions responsible for flow generation. Lymphatic vessels are divided into individual contractile units, termed lymphangions, which are separated by the valves and facilitate unidirectional flow [13].

Afferent collecting lymphatics carry the lymph to the lymph nodes. This lymph from the peripheral tissues contains antigens and antigen-presenting cells (APCs) from the downstream tissue and is important in facilitating local responses to infection as well as establishing self-tolerance [14]. Lymph undergoes significant modifications in lymph nodes due to the interactions of APCs with T-cells and due to hydrostatic and osmotic forces present in the lymph node capillaries [2, 15, 16]. As a result, the post-nodal lymph exiting the efferent collecting vessel has a higher count of lymphocytes [15] and proteins[16], while lacking APCs, most of which remain in the lymph node to present antigen to T-cells [17]. Efferent lymphatics carry the post-nodal lymph into the larger lymphatic trunks, e.g. thoracic duct, discharging fluid into the subclavian veins [18].

Movement of the lymph is facilitated by intrinsic and extrinsic forces [19, 20]. Intrinsic forces are generated by the contractions of the individual lymphangions [20], while the extrinsic forces induced by skeletal and other muscle contractions during physical movements, respiration, heart contractions, and intestinal motility [21, 22]. Such a system allows transporting the fluid from the limbs to the torso against the gravitational force and, under

normal conditions, prevent fluid accumulation in the interstitium [22].

Lymphatic endothelial cells are distinguished from blood endothelial cells in part by the expression of vascular endothelial growth factor receptor-3 (VEGFR3), the receptor that binds the growth factors VEGF-C and VEGF-D, which facilitate lymphangiogenesis [23, 24]. In addition, compared to blood endothelial cells LECs also express podoplanin [25], lymphatic vessel endothelial hyaluronan receptor 1 (LYVE-1) [26] a lymphatic-specific receptor for hyaluronan and prospero homeobox protein 1 (Prox-1), a transcription factor that play a key role in maintaining LEC identity [27].

LECs are connected through cell-to-cell junctions that are specialized depending in which part of the lymphatics they are present within: initial or collecting. In initial lymphatics, the cells possess junctions that have been described as "button-like", while in collecting vessels, they have a "zipper-like" phenotype. Different organization of cell-junction proteins creates these structures and facilitates fluid uptake from the interstitium into initial lymphatics and prevents its leakage from the CLVs. An adhesive protein vascular endothelial cadherin (VE-cadherin) along with several tight junction proteins comprise the "buttons", which alternate with the PECAM-1 (platelet/endothelial cell adhesion molecule-1) expression [28]. "Zippers" contain junctions that are similar to those found in veins, achieved through the continuous expression of VE-cadherin [29]. It was shown, that under the influence of elevated transmural flow, VE-cadherin and PECAM-1 were down-regulated and relocalized [30] which is thought to facilitate immune cell entry to initial lymphatics during inflammation. During the maturation of lymphatic vessels, zipper-to-button junction transformation occurs in initial lymphatics, while depletion of Angiopoietin-2 (*Agn2*) leads to leaky collecting vessels and impaired lymph uptake [31]. Thus the organization of junctional molecules within lymphatics is a dynamic process that has implications on both lymphatic development and the regulation of lymphatic permeability in health and disease.

1.2 Permeability

Lymphatic endothelial cells in initial lymphatics accommodate interstitial fluid absorption and keep the absorbed liquid within the vessel when interstitial pressure is below hydrostatic pressure within the lymphatic lumen. Chemical and physical factors, such as those that are elevated in high fat diet-induced obesity animal models, can account for increased permeability of the lymphatic vessels due to the change in the shape and cell junctions between the lymphatic endothelial cells [30, 32].

Lymphatic capillaries are highly permeable; therefore, the protein concentration of interstitial fluid is the same as the local initial lymphatics and there is minimal oncotic pressure gradient across the vessel wall. This observation is also true for the low-density lipoprotein (LDL) and high-density lipoprotein (HDL) levels in the peripheral tissues [33]. The collecting lymphatics are permeable to fluid and proteins (i.e., albumin) at a similar rate as venules [13, 34]. Thus there exists a small leakage of lymph from collecting lymphatic vessels due to the balance of Starling's forces (i.e. there is a minimal protein concentration gradient and larger transmural pressure compared to the initial lymphatics that favors fluid exit from the vessel and serves to concentrate lymph). However, this phenomenon does not affect the lymph transport to the lymph nodes, since only a small fraction of the liquid leaks into the interstitium under normal conditions [34].

However, this can change in pathologies such as cancer. Cancer induces not only angiogenesis through VEGF, but also lymphangiogenesis by production of VEGF-C, which forms leaky and disorganized blood and lymphatic vessels with abnormal function [35, 36]. This also promotes the migration of macrophages and leads to advancement of tumor metastasis [37, 38]. Leaky lymphatics are also associated with various disorders, such as atherosclerosis, obesity, and metabolic disorder type 2 diabetes mellitus [39]. Since adipose tissues are collocated around lymph nodes and collecting vessels, it was suggested, that lymphatics are permeable to lipids as well as to proteins [40]. Permeability of col-

lecting lymphatic vessels causes inflammation in prenodal adipose tissue (PAT) induced by inflammatory stimuli from the lymph and lymph-derived antigen presentation to the local PAT DC [41]. Conversely, obesity may induce lymphatic leakiness due to the chronic inflammation [42, 43, 44, 45, 46]. Furthermore, development of edema in the case of lymphatic obstruction or following a mechanical, chemical or thermal stimulus, has been associated with the increased permeability of the lymphatic wall [47].

Nitric oxide (NO) has a dual role in regulation of lymphatic permeability, depending on the state of the vessel. In wild-type collecting lymphatics NO increased the permeability, whereas in vessels from type 2 diabetes animals initial lymphatic barrier dysfunction was restored to normal [39].

Various inflammatory cytokines are known to increase permeability in blood vascular endothelial cells and for some their effect on lymphatic endothelial cells has been studied in-vitro. Specifically, cytokines TNF-α, IL-6, Th1-associated cytokines IL1-β, IFN-γ, and LPS all increased the permeability of an LEC monolayer grown on transwells [48]. Other *in vitro* studies performed on human dermal LECs treated with TNF-α for 24 hours revealed change in VE-cadherin distribution at the cell periphery and increased number of discontinuous cell junctions [49]. Inflammation also promotes lymphatic vessel enlargement and leakiness, while stimulation of the lymphatic vasculature with exogenous VEGF-C administration decreased this pathology in animals with rheumatoid arthritis [50]. At the same time, overexpression of VEGF-C leads to inflammatory macrophage chemotaxis and increased permeability [50, 51].

A few studies measuring lymphatic permeability *in vivo* revealed decreased lymphatic function, leakiness and up-regulation of VEGF-A upon UVB irradiation [52]. Most studies of lymphatic permeability have been conducted *in vitro*, and currently there are limited tools to induce spatially and temporally controlled alterations in lymphatic permeability. Inflammatory cytokines appear to be the most influential factors in increased lymphatic permeability together with neo-vascularization in tumors due to the overexpression of VEGF-

C [35, 36].

Thus, regulation of lymphatic permeability requires further research, including new approaches and animals models to quantify spatio-temporal fluctuations in lymphatic permeability over time.

1.3 Lymphedema

Lymphedema represents a group of pathological conditions, which manifest themselves as an excessive accumulation of interstitial fluid, caused by reduced lymphatic transport [53]. Such buildup of the protein-rich liquid causes inflammation, fibrosis, and adipose tissue formation [54]. Based on its origin, lymphedema can be primary or secondary [53].

Primary lymphedema may present itself at any point in life, from infancy to adolescence. It can be further classified based on the time it has been recognized: congenital lymphedema manifests itself within the first two years, while lymphedema praecox is diagnosed to patients undergoing puberty or in their 20s. However, primary lymphedema can also develop after 35 years and then commonly referred to as lymphedema tarda [53]. This type of lymphedema is rather rare, with an incidence of 1:100,000 across the globe [55]. Certain gene mutations are involved in the development of primary lymphedema. Mutations in the gene FOXC2 results in abnormal smooth muscle investiture surrounding the initial lymphatics and manifests in lymphedema distichiasis. Lymphedema distichiasis is characterized by lymphatic dysfunction, swelling of the limbs together with distichiasis, or extra set of eyelashes on the inner lining of the eyelid present at birth [56, 57] . Mutation of genes encoding VEGFR3 or VEGF-C results in Milroy disease, causing fluid retention due to either impaired fluid uptake by initial lymphatics or issues related to the lymphatic valve structure and functionality [58, 59, 60].

Secondary lymphedema is observed more frequently than primary. It occurs as a consequence of previous injury or obstruction of the lymphatic vessels, although there is some evidence that there may be an underlying genetic predisposition to developing secondary

lymphedema. Such lymphatic damage may be caused by filariasis, a parasitic infection, or as a result of injury, often initiated by lymph node dissection during the cancer treatment surgery or radiotherapy [55].

Lymphatic filariasis is a parasitic nematode infection responsible for most of the lymphedema cases worldwide. Approximately 120 million people are affected by this parasite in 83 countries, most of which are in tropical climate [61] and like wide-spread vector control. Mosquito vectors serve for larvae development and transmission to the human. First-stage larvae (microfilaria) from the blood is taken by the vector, in which it develops to infective larvae. Those larvae are transferred to the human host through the site of the vector bite and travel to the lymphatic vessels, where they grow into adult filarial parasites, which are able to reproduce for about 8 years [62].

The prevailing cause of secondary lymphedema in developed countries is cancer treatment. Nowadays, about 49% of cancer patients will be affected by secondary lymphedema following their cancer therapy [55] Radiotherapy, chemotherapy obesity, and lymph node resections, aimed to prevent the spread of the metastasis, are all positively correlated with increased lymphedema risk [63, 64].

Lymphedema is associated with significant changes in the local tissue environment. Since lymphatics are responsible for immune cell trafficking, impaired functionality results in the infiltration of macrophages, dendritic cells (DCs), and neutrophils at the site of lymphedema [44], resulting in chronic inflammation that drives tissue remodeling, retention of fat, development of fibrosis [42, 43, 44, 45, 46]. Local pressure changes often occur in the interstitium, resulting in impaired lymphatic filling. Another outcome of inflammation is enlargement of lymphatic vessels and their dysfunction [65, 66]. However, others have reported thickening of the lymphatic vessel wall, hyperpoliferation of lymphatic muscle cells, phenotypic “lymphoscleoris” or the narrowing of the vessel lumen due to this remodeling [67, 68].

Reduced lymphatic function, lymphatic remodeling and dilation of lymphatic vessels

could be caused by the inflammatory response of subsets of CD4+ T-cells, such as Th9, Th1, and Th17, Th2 cells [43, 69, 70]. Produced cytokines, such as IFN-γ and TNF-α have a potential to stimulate nitric oxide and, therefore, facilitate the progression of the lymphedema [69].

Furthermore, researchers have shown an increased count of regulatory T cells in the lymphedema limb in comparison with contralateral tissue in breast cancer patients [71]. A murine model of lymphedema, created through axillary lymph node dissection, revealed that upregulation of Tregs distal from the surgical site results in local immunosuppression, reduced tissue inflammation and inhibited lymphatic function. Depletion of the Tregs in this model restored the immune response in the local tissues [71].

Macrophages also increase following the ligation of lymphatic vessels in mouse models of disease. These cells also preferentially differentiate into M2 macrophages, which produce anti-inflammatory cytokines, and VEGF. However, the depletion of macrophage populations in lymphedema models also increased fibrosis and reduced lymphatic function. Additionally, VEGF-C expression was decreased and accumulation of CD4+ cells was observed [72].

While advances regarding the basic biology and immunology of lymphedema understanding has been limited primarily to preclinical animal models, current lymphedema treatment aims to prevent further progression through manual therapy, and lifelong treatment is required to manage the condition. One such treatment is a specialized form of massage referred to as manual lymphatic drainage (MLD). MLD therapy seeks to move fluid from the limbs and periphery to the torso via application of external pressure along lymphatic drainage basins with the motivation of moving interstitial fluid from an area of impaired lymphatic drainage to one where lymphatics are still functional [73].Compression garments are used to prevent fluid accumulation in arms and legs for an extended period of time [74]. Those procedures, together with physical exercise, comprise a daily routine of the lymphedema patients [75] and while helpful, patients remain desperate for a cure.

As there is no lymphedema cure available now, animal models are essential tools for understanding the disease and establishing the framework to discover a remedy.

1.4 Current animal models

Several animal models have been developed to replicate lymphedema and other lymphatic injuries and to further study this pathology and the remodeling of the lymphatic vasculature. The most frequently used animals for such studies are mice and rats. Those models can be divided into two groups: surgical and transgenic. Transgenic mouse models involve the embryonic of post-natal deletion of genes important in lymphatic development and maintenance. Examples of such models are the FLT4-DTR mouse expresses human diphtheria receptor (DTR) on its LECs, coupled to the lymphatic promoter FLT4 allows to ablate the lymphatics using the diphtheria toxin [76], K14-VEGFR-3-Ig mice (sR3 mice), where chimeric protein under a keratin-14 promoter secretes soluble VEGFR3 to neutralize VEGF-C and VEGF-D, inhibiting formation of the dermal lymphatic vessels [77], Prox1 haploinsufficient mice (Prox1+/-) [78], Chylous ascites-3 mutant mice (Chy-3) have depletion in chromosome carrying *Vegfc* and develop dermal lymphatic hypoplasia, penile and hind paws lymphedema [79]. Prox1 haploinsufficient mice that survive post-natal development (many die in utero or shortly after birth) develop obesity and have increased lymphatic permeability with the lymph leakage into the interstitium [42, 43, 44, 45, 46].

Several procedures are used to surgically induce lymphedema, particularly in rodent tails. Collecting vessels are present on both sides of the mouse's tail [80] and drain lymph from the tail to the external sacral lymph node [81]. To create lymphedema, a tail incision is performed, the collecting lymphatic vessels are cut and cauterized to create a flow blockage, and a gap of 2-3 mm in the skin is created to delay wound repair [82, 83], resulting in a highly repeatable swelling of the tail and pathology similar to lymphedema. The tail swelling and fluid accumulation are accompanied by increased lipid deposition and reduced collagen density in dermis a day after the incision, restored by day 14. At the

same time, hypodermis remains swollen, and its collagen density is elevated until, unlike clinical lymphedema, the pathology and swelling is restored by day 30 [82]. An alteration to this model was developed in which only one of the two collecting vessels is surgically damaged. This alteration allows one to study the adaptation and functional changes of the intact vasculature over the course of swelling [80]. Further models, while not an exhaustive list, include axillary lymph node dissection [84], hindlimb popliteal lymph node removal in sheep [85], and segmental resection of lymphatic vessels performed at the base of the rabbit ear [86].

Invasive models closely represent secondary lymphedema when the pathology is induced by surgery or injury. Lymphatic hyperplasia and dilation, abnormal lipid accumulation due to the leaky lymphatics and backflow, which have been observed in surgical models, leads to decreased lymphatic transport [82, 86]. Fibrosis develops in the subcutaneous and adipose tissues [46, 76]. Surgical animal models are acute due to the instantaneous response to the injury and usually self-resolve. Thus, they do not accurately represent the onset of human secondary lymphedema, which usually develops in months or years following the intervention and is a lifelong condition [55]. Therefore, the major disadvantage of secondary lymphedema models is the spontaneous resolution of the induced condition [87].

Surgical models do not only interrupt initial and collecting lymphatics, or remove the lymph node, but they also damage other local tissues. For that reason, the local immune response represents not only the lymphedema associated changes, but also consequences of tissues disruption. Novel animal models are required to understand the precise lymphedema pathology and chronology of its development. In addition, less invasive models are also needed to study the normal post-natal lymphangiogenic repair process and to understand when this process is adequate to return tissue homeostasis. To further investigate changes in lymphatic function upon localized injury, we propose to utilize a non-invasive photodynamic therapy approach, which preserves the skin integrity and targets the lym-

phatics, thus the use of this approach in different physiologic contexts both clinically and in mouse models is discussed further.

1.5 Photodynamic therapy. Verteporfin

Photodynamic therapy (PDT) is a clinical procedure, performed with the use of photosensitive drug and activating light. Once combined, this produces reactive oxygen species (ROS) and destroys targeted tissues, resulting in blood vessel occlusion [12]. Currently PDT is most commonly used clinically to treat various ocular neo-vascularization-related conditions, in particular age-related macular degeneration (AMD) [88]. Besides this, PDT is used to treat selected types of cancer, psoriasis and other dermatological conditions [89, 90, 91, 92].

Verteporfin is a photosensitive drug used in photodynamic therapy. It is a lipophilic molecule and is available on the market in a liposomal formulation, under the trade name Visudyne® (Visudyne®, Novartis Ophthalmics, Hettlingen, Switzerland). In Visudyne®, the active ingredient is encapsulated in liposomes, formulated with lactose, egg phosphatidylglycerol, dimyristoyl phosphatidylcholine, ascorbyl palmitate and butylated hydroxytoluene [93, 94]. This liposomal formulation was designed to increase the circulation of the drug upon IV delivery and slow its clearance.

1.5.1 Method of action

Being a two-stage process, photodynamic therapy requires not only administration of the drug, but also application of nonthermal red light. In photodynamic therapy, the photosensitizer absorbs the light energy and changes its ground singlet state S_0 to excited singlet state S_1. Excited triplet state T_1 arises from S_1 by intersystem crossing. In a type I reaction, it can directly induce photochemical reactions by generating cytotoxic free radicals, such as superoxide anions $O_2(-)$, hydroxyl radicals, hydrogen peroxide. In a type II reaction, the energy is transferred to the ground state oxygen triplet oxygen ($^3O_2$), forming excited state

singlet oxygen ($^1O_2$). This singlet oxygen causes photooxidation of the biological tissues. Both reactions may be present during the PDT, however singlet oxygen is considered to be the primary mechanism of the PDT induced damage, targeting enzymes, nucleic acids and causing cell death [95, 96].

Verteporfin has a wide absorption spectrum with multiple peaks (Figure 2.1). Clinically the wavelength used for excitation has been 689 nm, as this wavelength occurs near the optical window of tissues and can penetrate human skin to a depth of 5 mm, while 400 nm wavelength light reaches only 1 mm under the skin surface. This window is created due to the lower absorption of water, oxygenated, and deoxygenated hemoglobin at the wavelength range of 650 – 1350 nm [97, 98, 99].

1.5.2 Cell and tissue damage

Photodynamic therapy related damage occurs on several levels: cellular, immunological and vascular [95]. As it was mentioned before, immediate cellular destruction occurs due to generation of reactive oxygen species (ROS) [100]. The short lifetime of those oxygen molecules limits the damage to the exact area of the light activation, while keeping the surrounding tissues intact [95]. It has been suggested, that during PDT cells are more likely to undergo necrosis, if the photosensitizer is localized in the plasma membrane; and apoptotic cell death if the drug accumulates in mitochondria [89].

Vascular endothelium damage, particularly in intraluminal endothelial membranes is observed. This causes cytoskeletal structural rearrangement and endothelial cells shrinking. Following this, platelet binding is triggered due to the exposed vascular basement membrane. Consequently, histamine, tumor necrosis factor–α (TNF-α) and thromboxane are released by the activated platelets. This cases thrombosis, increased vascular permeability and vasoconstriction as well as further platelet activation. As a result, tissue suffers eventual hypoxia due to the blood flow stasis. Cytokine activity may also contribute to the blood vessel ablation, but another PDT effect on the immune system is reduced activity of

APCs at the low levels of the photosensitizer and light [95].

1.5.3 Previous studies of verteporfin effect on lymphatic vessels

Verteporfin effect on the lymphatic vessels has been investigated in a few studies. Due to its lipophilicity, verteporfin forms complexes with low-density lipoproteins (LDL) in blood stream and is preferentially taken up by endothelial cells through receptor-mediated endocytosis using low-density lipoprotein receptors (LDLR) [98, 101]. It has also been show, that LDLR is expressed on LECs of the collecting lymphatic vessels [102]. This property provides an opportunity for lymphatic vessels to be ablated similarly to the blood vessels, provided an appropriate method of delivery is used that targets lymphatic vessels. One such approach is to deliver the liposomal formulation of verteporfin (Visudyne®) via an interstitial injection under the skin as lymphatics actively drain large molecules from this area.

Upon light activation of the verteporfin, lymphatic endothelial cells undergo autophagy at low light doses of PDT and apoptotic cell death at higher doses [100]. Therefore, decellularization of the lymphatic vessel and basement membrane leads to their ablation and blockage of the transport of the lymph nodes [12, 103, 104].

Lymphatic vessels facilitate immune signaling and are involved in spreading of tumor metastasis even after the primary tumor is removed, as some tumor cells stay in the lymphatic vessels. In the first study, verteporfin was investigated as a potential method to destroy collecting lymphatic vessels associated with cancerous tumor and thus limit metastasis [103].

Cancer cells, which were implanted into the tip of the mouse ear, develop in-transit tumor nodules. Visudyne® was administrated intradermally in the ear periphery and was taken up by the lymphatics in the mouse ear, retained within the collecting lymphatics for 2 hours and eliminated from the ear skin within 48 hours following the injection. Application of non-thermal laser radiation of 689 nm at 3 to 5 mm from the injection site resulted in

fragmentation and death of lymphatic endothelial and smooth muscle cells. Following the procedure, dextran of high molecular weight was shown to leak out of the vessels, while control mock injection and irradiation did not lead to any changes. Following the PDT in the healthy mouse ear, no spontaneous regeneration of lymphatic vessels was detected during the 12-month observation, unless adenoviral delivery of VEGF-C was given to enhance regrowth [103]. However, lymphangiogenic factors released by the tumors could mitigate the PDT effectiveness in metastasis prevention [35, 36, 103]. Researchers examined the metastasis following the photodynamic treatment alone and coupled with an adenovirally expressed VEGFR-3 ligand trap (AdVEGFR-3-Ig) which inhibits lymphangiogenesis [103]. It was shown that the photodynamic therapy in combination with inhibition of lymphangiogenesis, prevented metastasis and transport of tumor cells though the lymphatic system. The ability of the photosensitizer to be taken up and retained in smaller lymphatic vessels causes less damage to the surrounding tissues, than occurs during surgery, making PDT an advantageous alternative to the surgical methods in cancer therapy. Preoperative photodynamic therapy of the mice flank in melanoma-bearing mice prevented metastasis and relapse in comparison with the control group, which did not undergo photodynamic therapy. Studies were also conducted in the pig knee, where termination of lymphatic drainage induced by the verteporfin was observed but required invasive delivery of a laser catheter to conduct the light activation. Liposomal verteporfin dosages used in these studies were 2 to 3 μl or 5 to 10 μl. Ophthalmological laser Zeiss Visulas 690S form Carl Zeiss Meditech or 680 nm red diode laser (Applied Optronics) were used to deliver light dose at 50 or 72 J/cm^2 at intensity of 600 mW/cm^2 [103].

Another study has shown that the light dose influences the lymphatic recovery time, while the drug dosage allowed one to target either both lymphatics and blood vessels or only lymphatics. In this study a light dose of 3.6 J/cm^2 blocked lymphatic drainage for about 1 week, with 25 J/cm^2 of light delivered the restoration took up to 3 weeks, while no adverse effects on blood vessels was present for either case. At the same time, the use of

0.4 J/cm^2 led to increased lymphatic permeability, but it did not occlude the vessel. The use of 100 ng verteporfin dose led to the destruction of both blood and lymphatic vessels. At the same time, the application of 25 ng and lower only showed effects on lymphatic vessels in the mouse ear dermis [12].

Finally, evaluation of the antitumor efficacy of verteporfin treatment in combination with antilymphangiogenic factors has been conducted. It was shown that elimination of the tumor associated lymphatics interfered with the development of anti-tumor immunity due to the decreased transport of the antigen-presenting DCs to the lymph nodes [105].

1.6 Lymphatic imaging techniques

Research of the lymphatic system has been complicated due to limited imaging options, which allow for non-invasive imaging with sufficient sensitivity and temporal resolution to distinguish lymphatic vessels [106]. Lymphangiography has been conducted since the early 1950s using radiopaque materials subcutaneously injected, taken into the small lymphatic vessels and imaged using X-ray. Similar approaches using labeled and contrast-enhanced tracers were developed for radiation-based imaging, such as computed tomography (CT) and positron emission tomography (PET) or PET-CT and single-photon emission computed tomography (SPECT) [107]. Magnetic resonance imaging (MRI) for the lymphatics imaging has also been developed. MR lymphangiography (MRL) has a potential in diagnosis or pre-procedure planning for the central lymphatic system (cisterna chyli, thoracic duct) [108]. MRL with subcutaneous injection of gadolinium provides an effective approach for imaging the lower extremity lymphatic vessels in patients with primary lymphedema [109]. Despite that, MRI is an expensive technology and there are safety concerns regarding the contrast agents. The main disadvantages are low spatial resolution, application limited to the thorax and retroperitoneum [107]. Because of these limitations, most of these techniques are used to map out local lymphatic anatomy, but provide limited information regarding lymphatic function.

Meanwhile, near-infrared (NIR) imaging allows one to study lymphatic vessel function *in vivo* with a non-invasive procedure using specific fluorescent dyes. NIR wavelengths ensures low light absorption and scattering in biological tissues and provides low autofluorescence, as it occurs in the optical window of tissues. Thanks to those properties, imaging lymphatics using NIR-labeled lymphatic-specific tracers provides images of superficial lymphatics with high spatial resolution and contrast [106, 110, 111]. Lymphatic specificity of the tracers is achieved through intradermal or subcutaneous delivery of tracers in the size range of 20 kDa up to 200 nm as these particles are too large to enter the blood vasculature but small enough to easily convect through the interstitial matrix.

Fluorescent lymphatic imaging is used to perform lymphatic mapping and intraoperative guidance. It is used to identify sentinel lymph nodes in breast and skin cancer patients during surgery as well as in non-invasive procedures for surgical planning [112, 113, 114, 115]. This technique also allows one to evaluate lymphatic drainage pathways [116].

Another application of NIR imaging is the evaluation of the lymphatic function. For example, one may compute the transit time of the dye from the injection site in the foot to the knee [117]. Also, contraction of the lymphatic vessels results in the appearance of fluorescent "packets", in which the fluorescence propagates along the lymphatic vessels. This has been observed in healthy patients and asymptomatic limbs of lymphedema patients, enabling one to quantify a metric of lymphatic function [106]. Several techniques for non-invasive quantification of the lymphatic transport and pumping function have been introduced for rodent models of lymphatic disorders [111, 118, 119, 120].

In most of the NIR imaging studies mentioned above indocyanine green (ICG) is used as a fluorescent tracer due to the fact that it has been FDA approved for other applications since the 1950s [106, 111, 112, 113, 114, 115, 116, 120]. When injected intradermally free ICG binds to proteins and is taken up by the lymphatics. However, a significant fraction of ICG was reported to also enter the blood vessels [119]. Also it was shown, that the repetitive administration of ICG leads to the decreased lymphatic function and enlarged

draining lymph nodes and thus may directly impair lymphatic function [118, 121].

Alternative tracers have attempted to resolve those issues: PEG conjugated NIR IRDye and ICG liposomes have been utilized for NIR imaging [119]. Both of those tracers are lymphatic specific and are not taken up by the blood vasculature [119] and do not inhibit lymphatic function [118]. Liposomal ICG has the potential to target selected cells by incorporating antibodies or the surface ligands [122]. Further improvements to NIR based imaging techniques and evaluation of lymphatic function will allow one to expand the clinical application of this technique.

Over the years, multiple animal models have been developed to study lymphedema and lymphatic physiology. While transgenic animals exhibit a systemic effect of the mutations and high morbidity, invasive procedures result in acute swelling followed by its spontaneous resolution and, therefore, differ from those of clinically observed secondary lymphedema. Moreover, surgical manipulations cause localized tissue damage, making it difficult to distinguish between wound healing and lymphatic regeneration. Therefore, there is a need for non-invasive techniques to induce localized disruption of lymphatic vessel integrity and to study to the resulting adaptations in lymphatic function to such injuries. In this work, we sought to investigate the potential of verteporfin-based photodynamic therapy to induce such an injury in the mouse tail. This location was chosen as it is well established in lymphedema studies and allows for lymphatic function evaluation using NIR imaging.

CHAPTER 2

EVALUATION OF LONGITUDINAL LYMPHATIC FUNCTION CHANGES UPON INJURY IN THE MOUSE TAIL WITH PHOTODYNAMIC THERAPY

2.1 Introduction

The lymphatic system is responsible for fluid homeostasis[2], immune cell trafficking[3] and lipid transport[1]. Protein-rich fluid from the interstitial space is transported unidirectionally to the blood circulation in the form of lymph [4]. This liquid is collected by initial lymphatics and transported to pre-collecting lymphatics where it is then transferred to collecting lymphatics, which lead to lymphatic trunks or ducts and eventually return the fluid into the blood circulation [4]. While significant strides have been made over the past few decades understanding the molecular mechanisms important for lymphatic development, our understanding of postnatal lymphangiogenesis in health and disease is in its nascent stages. New animal models of lymphatic injury will thus provide useful experimental platforms for further exploring lymphatic post-natal adaptation in health and disease.

Photodynamic therapy is widely utilized for anti-tumor treatments, age-related macular degeneration and various dermatological conditions, such as psoriasis and vitiligo [91]. This technique is based on photosensitizer activation with non-thermal light, which leads to generation of reactive oxygen species (ROS) [12, 95]. One of the drugs widely used for this purpose is Visudyne®(Novartis Ophthalmics, Hettlingen, Switzerland), a liposomal formulation of verteporfin. This technique has been particularly effective for disrupting newly formed vasculature, where intravenously delivered drug in concentrated in cells with a high density of low-density lipoprotein receptors (LDLR) which assist in the endocytosis of the drug [95]. Since the drug has been on the market for 20 years, it has been extensively

studied with regards to its effect on blood vasculature [90, 91, 92, 95].

In recent years lymphatic-specific photodynamic therapy using verteporfin has been explored in the context of the prevention of tumor metastasis [103]. Scientists have also investigated lymphatic regeneration following PDT in the mouse ear [12] and investigated the effect of PDT in combination with lymphangiogenesis inhibition on anti-tumor immunity [105]. However, it is unclear how the generation of ROS during PDT alters lymphatic function and whether this method can be used to disrupt lymphatic function in tissue beds where the skin is thicker than the mouse ear. Lastly, while verteporfin is usually used in a liposomal formulation, which was designed specifically to slow its clearance from the blood circulation, it is has not been established whether free intradermal delivery of verteporfin may be used for lymphatic-specific PDT.

Thus the aims of this study were to (1) establish whether photodynamic therapy-induced lymphatic injury may be developed in mice tail using non-liposomal verteporfin formulation and an NIR imaging system without laser irradiation, and (2) evaluate changes in lymphatic function following PDT using non-invasive imaging techniques.

2.2 Materials and Methods

2.2.1 Verteporfin and its activation using NIR

Verteporfin was obtained from Sigma-Aldrich (St.Louis, MO, USA). The powder was stored protected from light at -20°C. Since the chemical is not water-soluble, it was reconstituted using DMSO warmed to 37°C at a concentration of 2 mg/ml and aliquoted for future use. To dilute the reconstituted verteporfin, 5% dextrose solution was used, as precipitation in saline solutions may occur [123].

The drug solution was injected intradermally (ID) into the tail tip at a volume of 10 μl. During preliminary studies dosages of 200 $\mu g/ml$, 400 $\mu g/ml$, 600$\mu g/ml$ were tested out (n=4). For these experiments, corresponding doses of DMSO in 5% dextrose solution were used as a vehicle control to ensure that no DMSO-related effects were present. The dosage

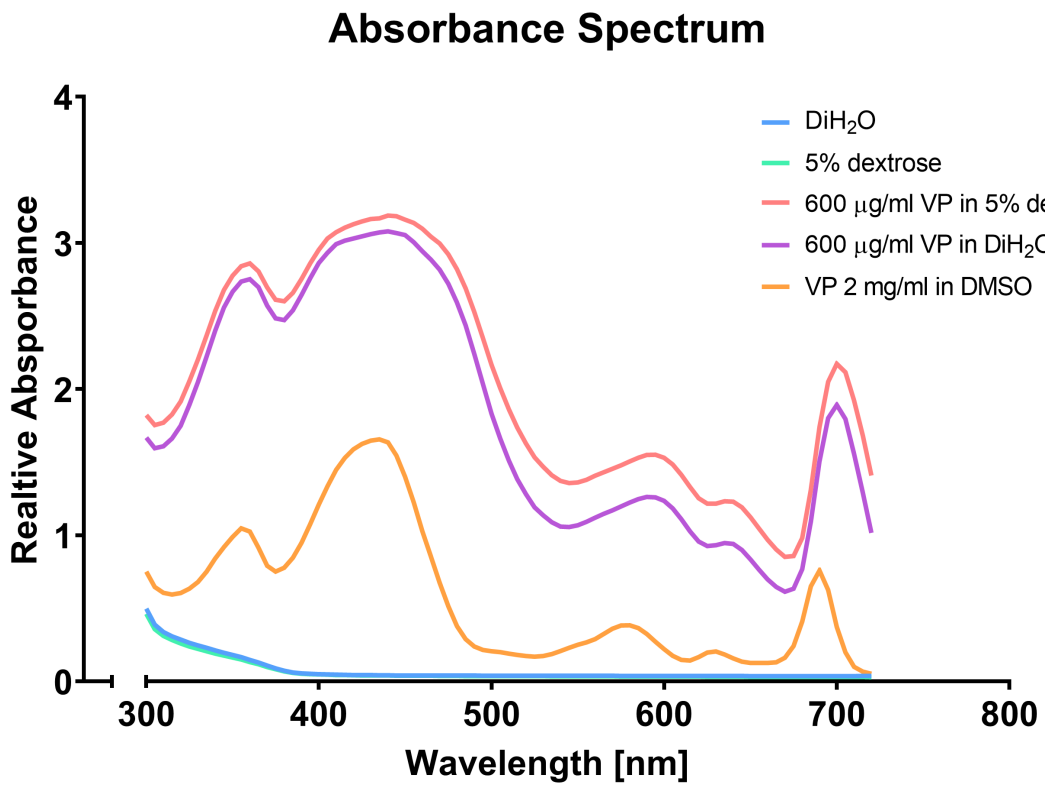

Figure 2.1: Absorbance spectrum of verteporfin in various solvents. Distilled water, and 5% dextrose have the same absorbance spectrum. 600 $\mu\mathrm{g/ml}$ verteporfin solution in 5% dextrose was used for the injections. Verteporfin 2 $\mathrm{mg/ml}$ in DMSO represents initial stock solution, used to create the final dilution.

of 600 $\mu g/ml$ was used for the remainder of the experiments, as it caused visible changes within the targeted area within 2 days as confirmed by NIR imaging.

In this study, a customized dual-wavelength NIR imaging system was used to both image the lymphatics with a lymphatic-specific tracer and to induce photosensitizer activation by the light. Specifically, a Cy5.5 filter set (49022-ET-Cy5.5, Chroma Technology Corp, VT, USA) was used: excitation filter ET650/45x with a center wavelength of 650 nm and 45 nm full width at half maximum (FWHM), dichroic beam splitter T685lpxr, and emission filter ET720/60m, where the center wavelength is 720 nm, and FWHM is 60 nm. According to the Visudyne® prescription information for ophthalmological use, recommended light dose for treating neovascular lesions is 50 J/cm^2 with an administration intensity 600 mW/cm^2 for 83 s [93, 123]. To determine the power delivered through the Cy5.5. filter set

to the site of application, the power was measured at various magnifications by adjusting the objective optical zoom and using the Thorlabs photometer PM 10-3 (Thorlabs, Newton, NJ). As the zoom is increased, the lens distributes the available power over smaller area. As it is presented on the Figure 2.2, measured power initially increased with increased magnification as the light from the excitation source become completely contained within the photodetector surface and then slowly decreased with increased magnification, indicating that the some power is lost through the objective as the focus is further increased.

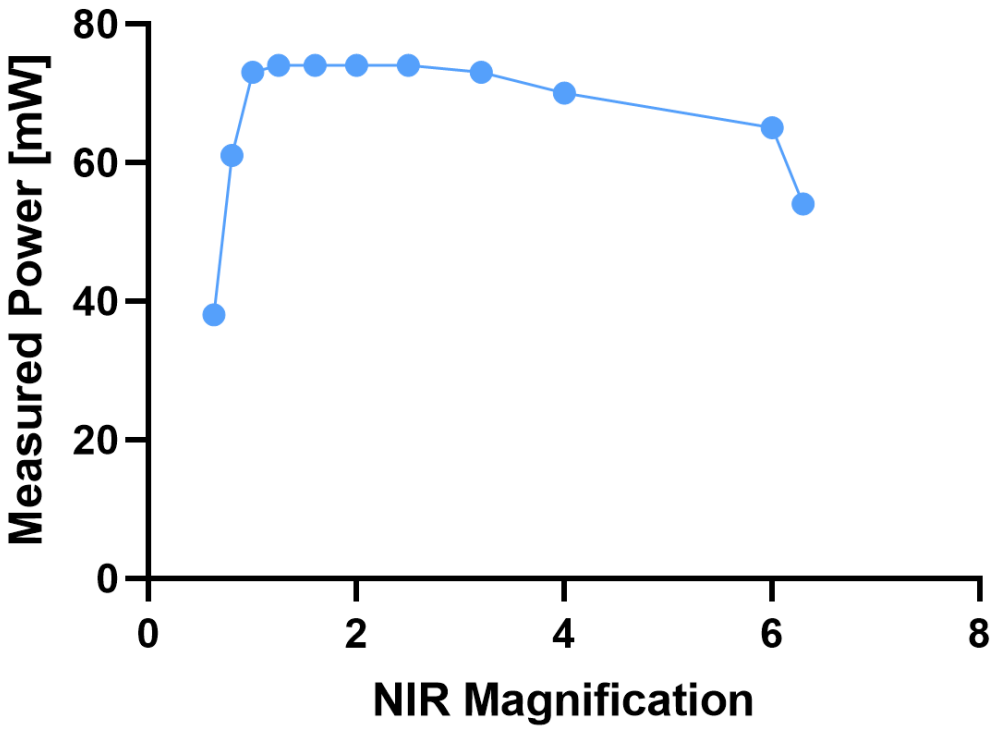

Figure 2.2: Power output for the Cy5.5 NIR filter at various magnifications.

We chose the maximum optical zoom of 6.3X as the light fluence was maximum here due to the minimal illumination spot size. In addition, the size of the light beam at this magnification allowed us to focus the beam on a specific surface of the tail of about 0.2 cm^2. The light fluence achieved under these settings was estimated using the following

equation:

$$Light fluence[J/cm^2] = \frac{Power Density[W/cm^2] * Time[s]}{1000}$$

The power density of 275 mW/cm^2 was estimated based on the laser beam area in focus, which was a circle with approximately a 5 mm diameter (area of 0.19635 cm^2). From the equation above, an exposure time of 179 s would achieve a fluence of 50 J/cm^2, while 258 s would achieve 72 J/cm^2, discussed in previous studies [103].

2.2.2 PDT in the mouse tail

Experiments were conducted on C57BL/6 mice 6-10 weeks old. Animals were separated into two groups of 8, each comprising 4 male and 4 female mice. Animals were anesthetized with 5% isofluorane and kept under 1.9% isoflurane for the experiment's duration. Mice body temperature was maintained around 37°C. Verteporfin was resuspended in DMSO, as described above, and prepared with 5% dextrose to achieve the desired concentration of 600 $\mu g/ml$ and volume of 10 μl. During the first 5 minutes of injection the tail was protected from light by covering it with aluminum foil. Then the targeted area was irradiated with a focused beam of 0.2 cm^2 to achieve verteporfin activation for 5 minutes on the top, right and left sides at a distance 4.5 cm from the tail tip to induce lymphatic injury on the vessels at this location. The exposure time of 5 minutes provided the fluence of 82.5 J/cm^2 at every side. This increased exposure time of 5 minutes (compared to other published studies) was motivated by the greater tissue thickness and more absorption and scattering of the light by the tissue of the mouse tail than in occurs in ophthalmological applications or in mouse ear dermis. The light delivered through our filter set is also off peak from the local absorption maximum of 700 nm, although the absorbance at 650 nm is within 50% of this peak value.

The schematic representation of the experimental set-up is shown on Figure 2.3.

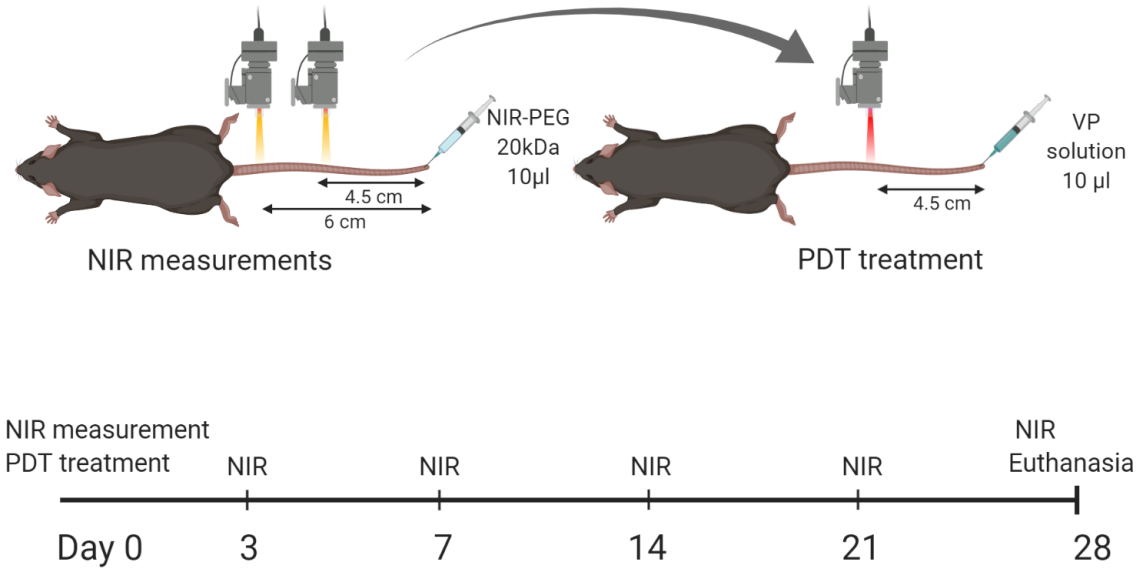

Figure 2.3: Experimental set-up. NIR measurement of lymphatic function were made prior to verteporfin treatment to establish baseline measurements of lymphatic function on day 0. Verteporfin was then administered intradermally in the tail tip, and the tail was exposed to light for the activation as described in the methods (or left unexposed in control mice). Mice received follow on measurement of lymphatic function 3, 7, 14, 21, and 28 days after the initial injury. Figure was created with BioRender.com.

2.2.3 NIR Imaging

Lymphatic contractility function was evaluated *in vivo* in mice tails with NIR imaging using previously described techniques [111, 119, 120].

20kDa polyethylene glycol (PEG) was conjugated with IRDye 800CW NHS Ester (LI-COR Biosciences) to synthesize the lymphatic specific tracer. PEG is dissolved in DMSO with NIR dye at a dye to PEG ratio of 1:1.5 and mixed on a shaker for 24 hours, then transferred to dialysis cassette that has the molecular weight cut-off of 7 kDa for its semi-permeable membrane (Slide-A-Lyzer, ThermoFisher Scientific). This cassette enables the free diffusion of small molecules and retains the larger molecules on the sample side of the membrane and was placed into the distilled water for 24 hours of dialysis, aliquoted and lyophilized. The final dye is stored at -20°C and resuspended in 0.9% saline (sodium

chloride) for injections [124]. 10 μl of tracers is administered intradermally into the tail tip of anesthetized mice immediately prior to imaging.

The NIR imaging system, along with MicroManager software, was used to collect the images. The system consists of stereo-microscope MVX10 (Olympus) with an attached electron-multiplying charge-coupled device (EMCCD) camera (Evolve eXcelon, Photometrics) and xenon arc lamp light source with automated shutter controller LB-LS/30IR (Sutter Instrument Company). The microscope is also equipped with two sets of NIR excitation and emission filters, the Cy5.5 filter set described above, and a second NIR filter set for imaging the lymphatic PEG tracer: a 769 nm bandpass excitation filter with 49nm FWHM (Brightline FF01-769/41-25 25MM, Semrock), an 832nm nm bandpass emission filter with 45nm FWHM (Brightline FF01-832/37-32 32MM, Semrock) and an 801.5 nm longpass dichroic mirror (Brightline FF801-DI02-32X44-XL, Semrock) [80, 124].

The field view for the functional measurement was centered at the same location as the site of the verteporfin activation on the mouse's tail, 4.5 cm from the tail tip. After injection of the tracer, the lymphatic contractile function was recorded for 5 minutes from the top view of the mouse. Then, the left and right sides of the tail were imaged for the same period by placing the mouse on its side. NIR exposure time on the camera was set to 50 ms with a frame rate of 10 fps. NIR functional analysis to determine the packet frequency, packet amplitude, and packet has been described previously [80]. An ROI containing the collecting vessel is selected and the spatially averaged intensity change over time within the ROI is obtained and used to calculate the functional parameters.

Discrete packets of fluorescence are observed when the lymph moves through the lymphatic vessels due to the intrinsic contractions and operation of the lymphatic valves [120]. Packets frequency has previously been established as a measure of the lymphatic function by counting the number of contractile events [111]. The amplitude of those packets corresponds to the contraction amplitude of the vessel [80, 125]. Here this parameter is evaluated as a percentage difference between the maximum and baseline intensity of the

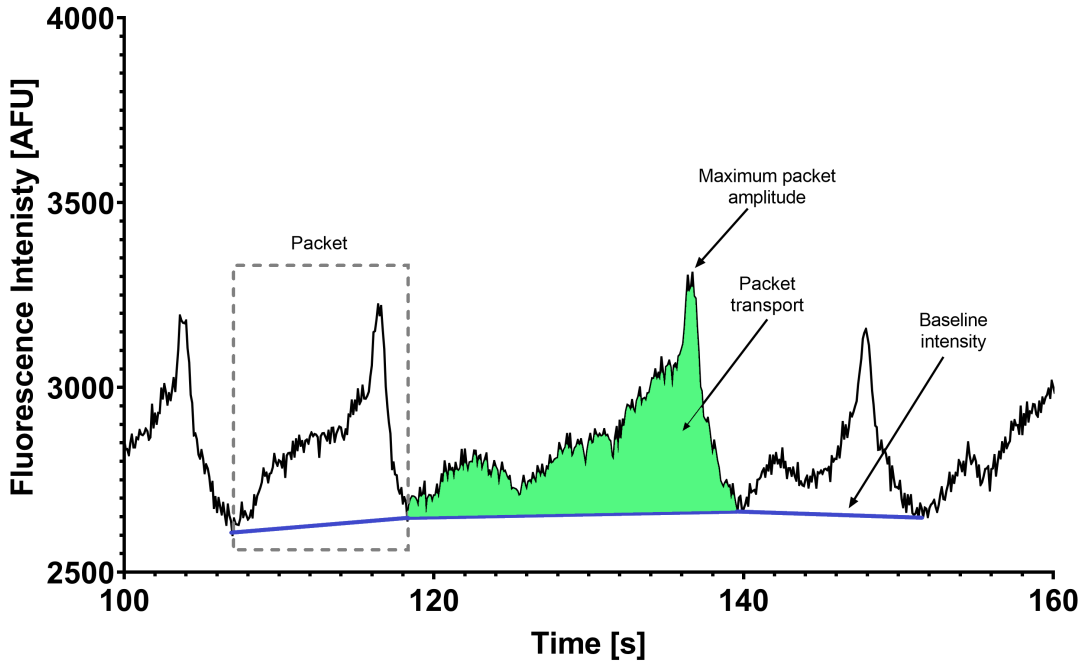

Figure 2.4: Lymphatic function evaluation. An example packet of fluorescence is highlighted in the gray box. Packet frequency is the number of packets observed per minute. Amplitude percentage difference is calculated as the difference between maximum packet amplitude and baseline intensity divided by baseline intensity at the given timepoint. The baseline intensity line connects the minimum intensity values of the packets. The packet transport is calculated as the area under the curve normalized to the base line intensity, summed over all of the packets and divided by the total time. Area under the curve is calculated as sum differences between the intensity and baseline values for each timepoint within the packet. In results we report the packet transport normalized to the baseline intensity at every given point.

packet divided by the baseline signal intensity at the given time to adjust for the brightness and averaged across the measurement time (Figure 2.4). Packet transport is calculated as an integral of the packet frequency over time and represents the fluorescence transport driven by intrinsic contraction [126], it is also normalized to the baseline intensity.

$$PacketTransport = \frac{\sum_{i=1}^{n} \int_{t_1 i}^{t_2 i} \frac{f(t)-g(t)}{g(t)} dt}{time}$$

Where n is number of packets in the measurement, $f(t)$ is fluorescent signal within the packet region, limited by minimum $(t_1 i)$ and maximum $(t_2 i)$ time points of each packet,

$g(t)$ is baseline intensity within the packet.

During the follow-up measurements, if distinct collecting vessels were not visible at the treatment area, additional data accusation was completed proximal to this area at approximately 6 cm from the tail tip. All data for each animal is reported as the average of four ROI measurements: left and right sides of the tail with two vessels within each location.

2.2.4 Quantification of lymphatic leakage

To evaluate the amount of dye that had leaked out at the injury site, image processing techniques were applied. The first step was the identification of the mouse tail. Percentile based filtering was proven to be the most effective for this task.

The distribution of intensities within the image is used for this evaluation. The function identifies the intensity at which 72% of the pixels in the image have lower fluorescence than the top 28%. These pixels are set to a zero value, while the other 28% remain unchanged. This percentile was selected based on the assumption that the tail occupies a relatively consistent area of the image in a given video sequence. This final value was selected through multiple runs across a random selection of mice.

Segmentation of the dye within the tail was based on the calculating the mean intensity within the tail and selecting 20% of the brightest pixels above the mean.

The code was developed by using Python, including optimized libraries, such as NumPy and SciPy. Therefore, this code can be executed on various operating systems as an open-source tool and is included in the appendix.

2.2.5 Statistical analysis

To evaluate the effects of time since injury, and the effect of light activation of verteporfin, non-parametric paired and unpaired tests were performed to determine the statistical significance of the results. Mann-Whitney test was used to compare difference between two animal groups, while Wilcoxon test identified significant changes from the baseline mea-

surements. Two-way ANOVA was applied to evaluate lymphatic function change on day 7 in animals of different gender. Tuckey's multiple comparison test was performed following ordinary one-way ANOVA to evaluate the effect of verteporfin based treatment downstream from the injury location. A Shapiro-Wilk test was performed to test for normality, and while most of the data for the groups was normally distributed, there were some exceptions likely due to the small sample size. All statistical computations were performed using GraphPad Prism 8.4.3.

2.3 Results

2.3.1 Automated tail and dye detection

Examples of the tail and dye detection algorithm are represented on Figures 2.5 and 2.6. Unlike surgical injury of the mouse tail lymphatics, there was no detectable tail swelling in these animals (Figure 2.7 A). In animals with the low overall fluorescence levels, the tail thresholding included some pixels as positive that can clearly be seen to be in the background upon visual inspection. However, this small amount of noise did not influence the estimation of the tail size and was not observed for the animals with higher fluorescence intensity within the tail.

Under normal conditions, the tracer is taken up by initial lymphatics at the injection site and transported downstream within collecting lymphatics such that only collecting lymphatics are visible at the imaging site (Figure 2.5, Figure 2.6 A,B). Control mice presented with clear anatomically distinct collecting lymphatic vessels during all of the follow-up days. PDT treated mice exhibited leakage of tracer out of the collecting vessels and often showed uptake into the surrounding hexagonal initial lymphatic network. When these images were quantified, there were no significant differences between the baseline and the follow-on days in the measurement of dye distribution in verteporfin-only animals. In PDT treated mice, such changes were observed. Specifically, the fluorescent tail area percentage significantly increased on day 7 18.322 ± 9.597, day 14 18.999 ± 11.156, day 21

18.204±16.563 and day 28 14.910±10.789 post procedure in comparison with the baseline measurement 7.315±2.725 (mean±SD) (Figure 2.7 B).

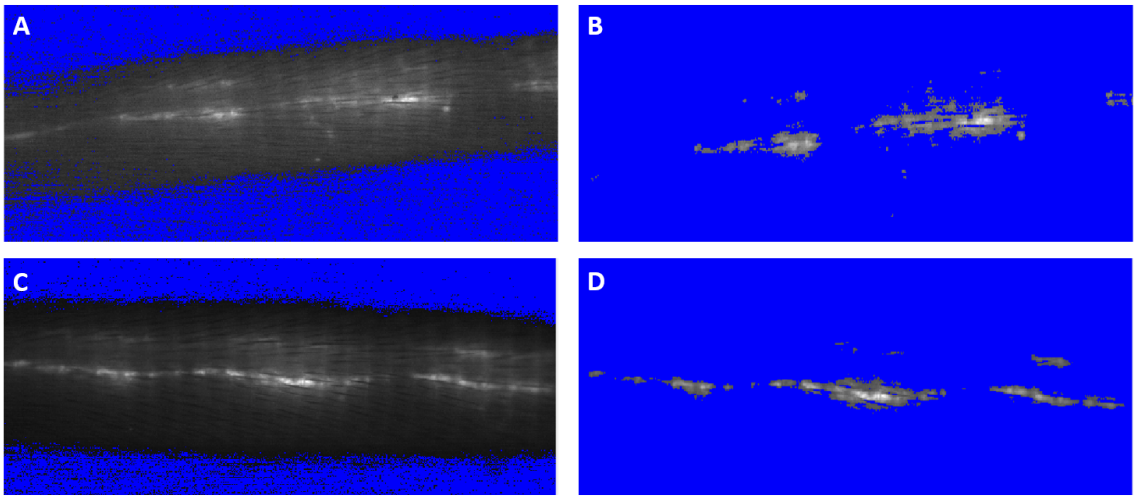

Figure 2.5: Example of tail and dye detection in verteporfin only group (control group). Top row represents the baseline day 0 measurements, bottom row represents day 3 follow-up. (A,C) Results of the tail detection algorithm, (B,D) fluorescent area.

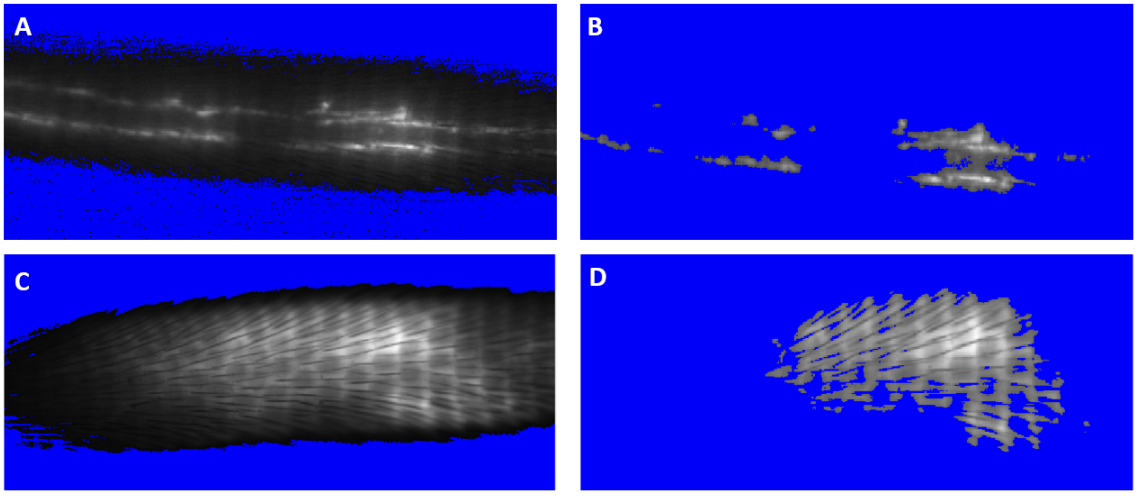

Figure 2.6: Example of tail and dye detection in verteporfin with light activation group (PDT group). Top row represents the baseline day 0 measurements, bottom row represents day 3 follow-up. (A,C) Results of the tail detection algorithm, (B,D) fluorescent area.

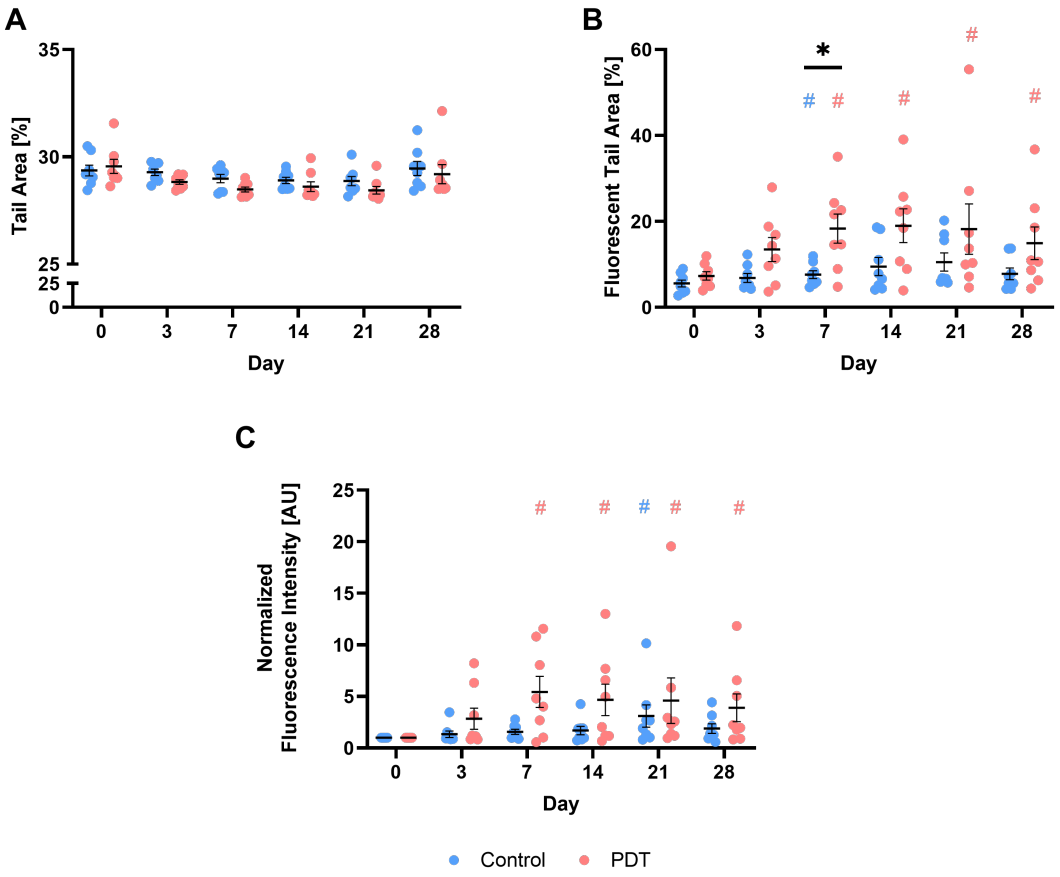

Figure 2.7: Lymphatic PDT result in increased dye leakage from lymphatics at the site of injury. (A) Image area occupied by the tail was evaluated as a detected number of pixels over the total number of pixels in the image. There were no detectable changes in tail size between either group over the 28 day period. (B) PDT treated animals developed an increase in the tail area with fluorescence tracer above background, indicating dye leakage at the site of injury, while statistical differences were also observed in the control group (verteporfin only) on day 7 in comparison with baseline measurement. (C) There were significant differences in brightness at the imaging site in comparison with the baseline measurement, where the intensity was consistently higher for the PDT group. No statistically significant differences were observed between control and PDT groups, suggesting that while enhanced leakage was occurring, the lymphatic tissue bed was still capable of clearing the dye. Significance on this graph is shown for the comparison of each day to the baseline measurement within the study groups using Wilcoxon test. *represents a statistically significant difference determined by Mann-Whitney test: comparison between animal groups at the given time point. # represents a statistically significant difference determined by Wilcoxon test: comparison with the baseline measurement of the same animal group. #$P<0.05$, n=8 for both animal groups. Error bars represent mean$\pm$SE

Tail and fluorescence area detection was completed using automated image processing. Since every measurement contained a few thousand images, their averages were used to report the results. From this, the data for each side of the tail was obtained (Figure C.1). Considering that observed trends were similar between the sides, right, left, and top side measurements were averaged for every animal (Figure 2.7).

2.3.2 Lymphatic function changes following the PDT

Several measures of lymphatic function parameters were significantly decreased after PDT treatment (Figure 2.8). Particularly, a statistically significant difference in normalized packet frequency between PDT 0.334 ± 0.625 and control 1.333 ± 0.448 groups was observed on day 7. This parameter also significantly decreased in comparison to the baseline values in PDT group on day 3 0.353 ± 0.616 and day 7 (Figure 2.8 A). Normalized packet transport, which is a measure of the fractional pump flow due to contraction, for PDT mice significantly changed on day three 0.328 ± 0.466, day 14 0.2 ± 0.248 and day 28 0.396 ± 0.524 in comparison with the baseline, while for control mice such change occurred only on day 28 0.542 ± 0.265. Statistically significant difference between PDT 0.200 ± 0.248 and control 0.646 ± 0.455 animal groups was present on day 14 (Figure 2.8 B). Packet amplitude, which is indicative of contraction amplitude of the vessel wall, was statistically different from the baseline measurement for PDT treated animals on day 3 0.254 ± 0.36, day 7 0.393 ± 0.683, day 14 0.195 ± 0.318, and day 28 0.348 ± 0.435; for control animals on day 28 only 0.667 ± 0.346. Normalized packet amplitude was also significantly different between PDT and control groups on day 3 and day 14, when the values for control group were 0.903 ± 0.885 and 0.747 ± 0.398,respectively (Figure 2.8 C). All the values above represent mean$\pm$SD.

As a general trend, after day 14, lymphatic function in PDT treated animals returns close to the baseline levels after a transient loss of function early on. At the same time, the function in control mice remains consistent throughout the experiment.

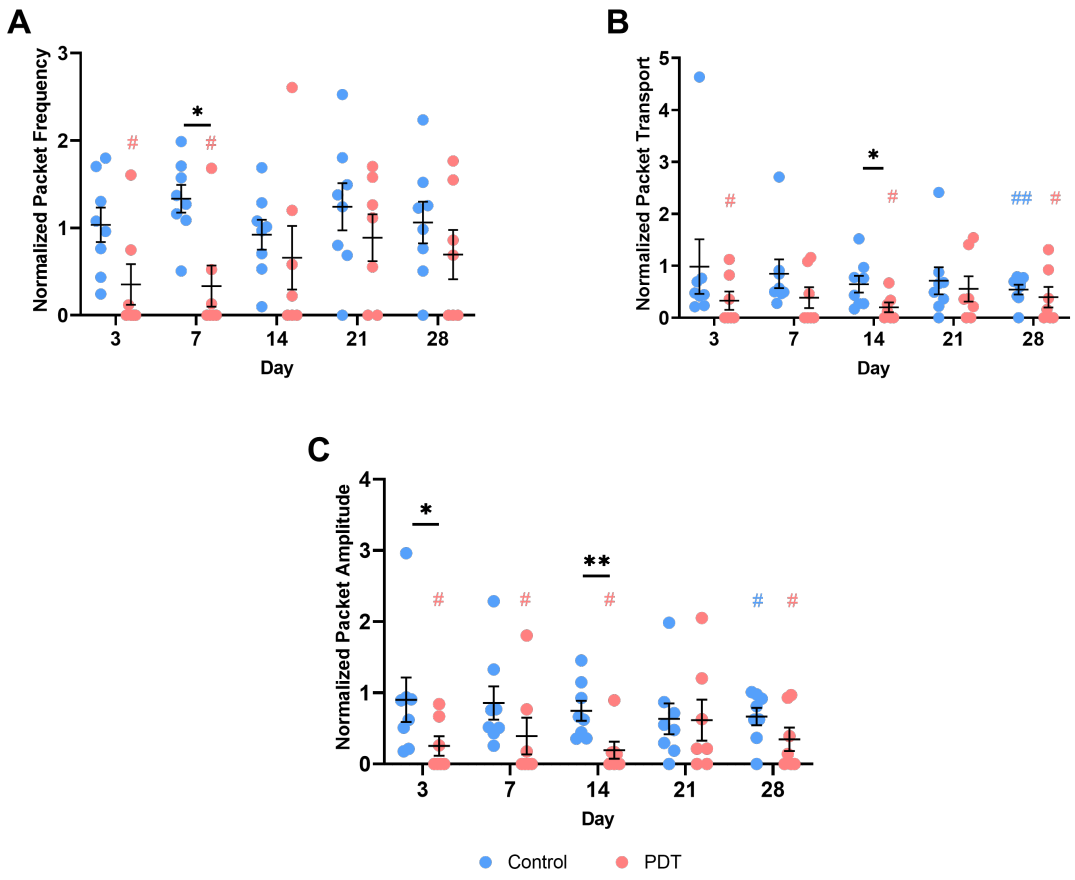

Figure 2.8: Lymphatic function decreased over time in PDT animal group. Parameters of lymphatic function throughout the study. (A) Packet frequency for PDT was less than control one week following the procedure, while no statistically significant differences were present between PDT and control in following weeks. (B) Normalized packet transport significantly decreased from baseline values on days 3, 14, and 28 for the PDT group while for the control group there was a statistically significant decrease in packet transport at day 28. Between two groups statistically significant difference was observed on day 14. (C) Packet amplitude was significantly lower in PDT group on days 3, 7, 14, and 28 post-treatment while in control group statistically significant differences in packet amplitude was observed on day 28. Control and PDT group presented statistically significant differences on days 3 and 14. *represents a statistically significant difference determined by Mann-Whitney test: comparison between animal groups at the given time point.# represents a statistically significant difference determined by Wilcoxon test: comparison with the baseline measurement of the same animal group. *P$<$0.05, **P$<$0.01, #P$<$0.05 ##P$<$0.01, n=8 for control group, n=7 for PDT group. Error bars represent mean$\pm$SE.

As significant differences between the two animal groups were observed on day 7, we used this day to complete further comparison between genders and to study the lymphatic

function proximal and downstream to the injury site.

2.3.3 No gender differences in function as injury response

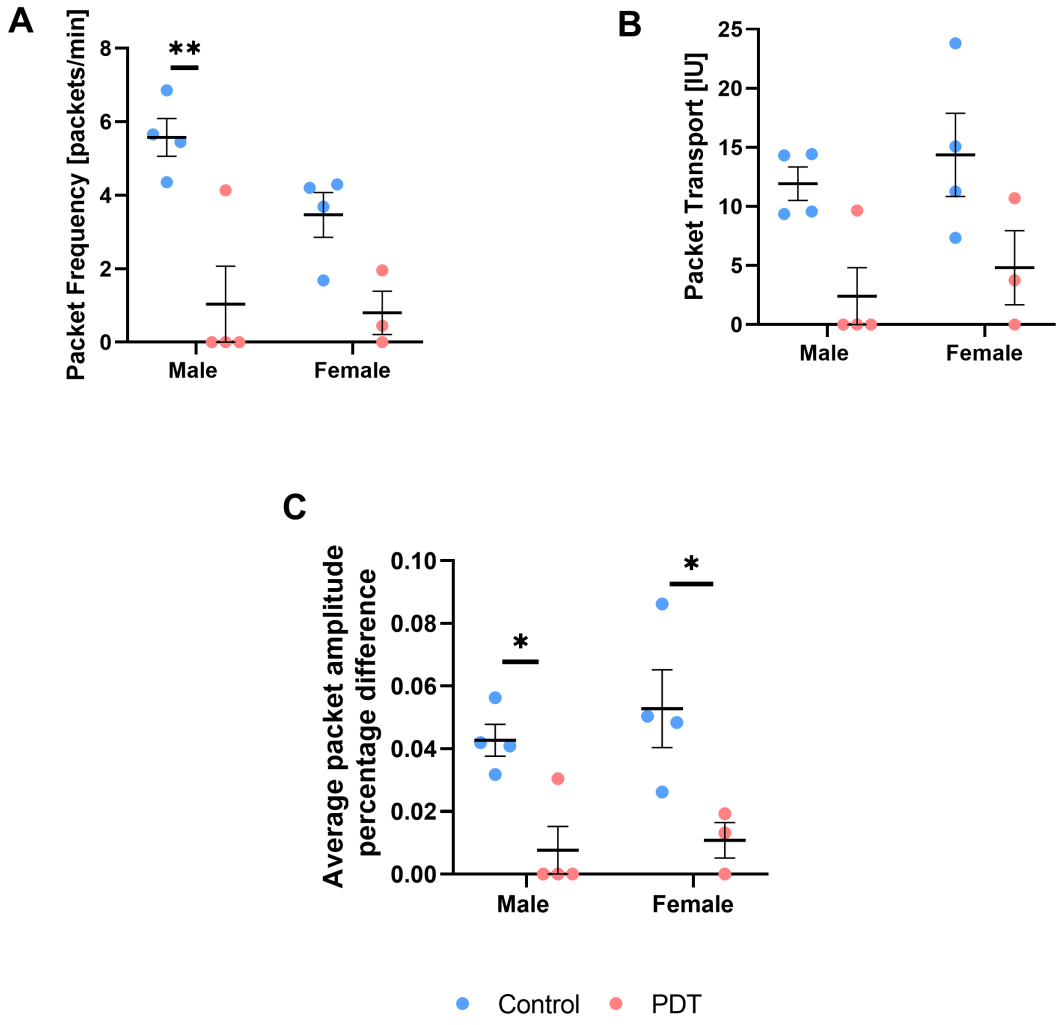

Figure 2.9: Verteporfin treatment outcomes are independent of animal gender. Lymphatic function evaluated on day 7 presents difference between verteporfin only and light activated animal groups. *P$<$0.05, **P$<$0.01, n=8 for control group, n=7 for PDT group. Error bars represent mean$\pm$SE.

Given the increase prevalence of lymphedema in women compared to men, we sought to determine if there were gender differences in the response to injury. Both male and female mice were used in the study and the effect of gender on the results was investigated on

day 7, when significant changes due to PDT therapy were observed. Photodynamic therapy treatment provided an equal effect on both male and female mice, with PDT decreasing lymphatic function across all measures at this timepoint (Figure 2.9).

2.3.4 PDT alters lymphatic function in downstream lymphatics proximal to the injury site

To determine if the loss of lymphatic function occurred only at the exact site of light activation, or if its effects could be propagated to lymphatics downstream, we imaged lymphatic 7 days after surgery 6 cm from the tail tip (Figure 2.10). Downstream of the injury there were significant reductions in function compared to the control group for most functional parameters, however, there was no difference for packet frequency. There was also no difference in function between the site of light activation and the site further downstream.

Specifically, packet frequency [packets/min] was significantly lower for the PDT animal group at the injury site 0.934 ± 1.582 in comparison with verteporfin only 4.523 ± 1.538 (Figure 2.10 A). Packet transport [IU] was significantly decreased for the animals with verteporfin activation at the site of the light application 3.443 ± 4.807 and proximal from it 4.316 ± 7.072 in contrast to the verteporfin without light activation group 13.146 ± 5.133 (Figure 2.10 B). The same trend was observed for the average packet amplitude percentage difference, where amplitude for verteporfin only 0.048 ± 0.018 was significantly greater than for PDT injury site 0.009 ± 0.012 or PDT at 6 cm from the tail tip 0.016 ± 0.022 (Figure 2.10 C). Values above represent mean$\pm$SD. Number of animals in the verteporfin treatment (PDT) downstream was 5 as oppose to 7 animals in PDT group and 8 animals in control group.

As a result, it was shown that photodynamic therapy can be administered and longitudinal function imaged using a dual-wavelength NIR stereomicroscope system and intradermal delivery of non-liposomal verteporfin. This treatment resulted in increased lymphatic permeability and loss of lymphatic contractile function, which peaked one week after injury and resolved within one month.

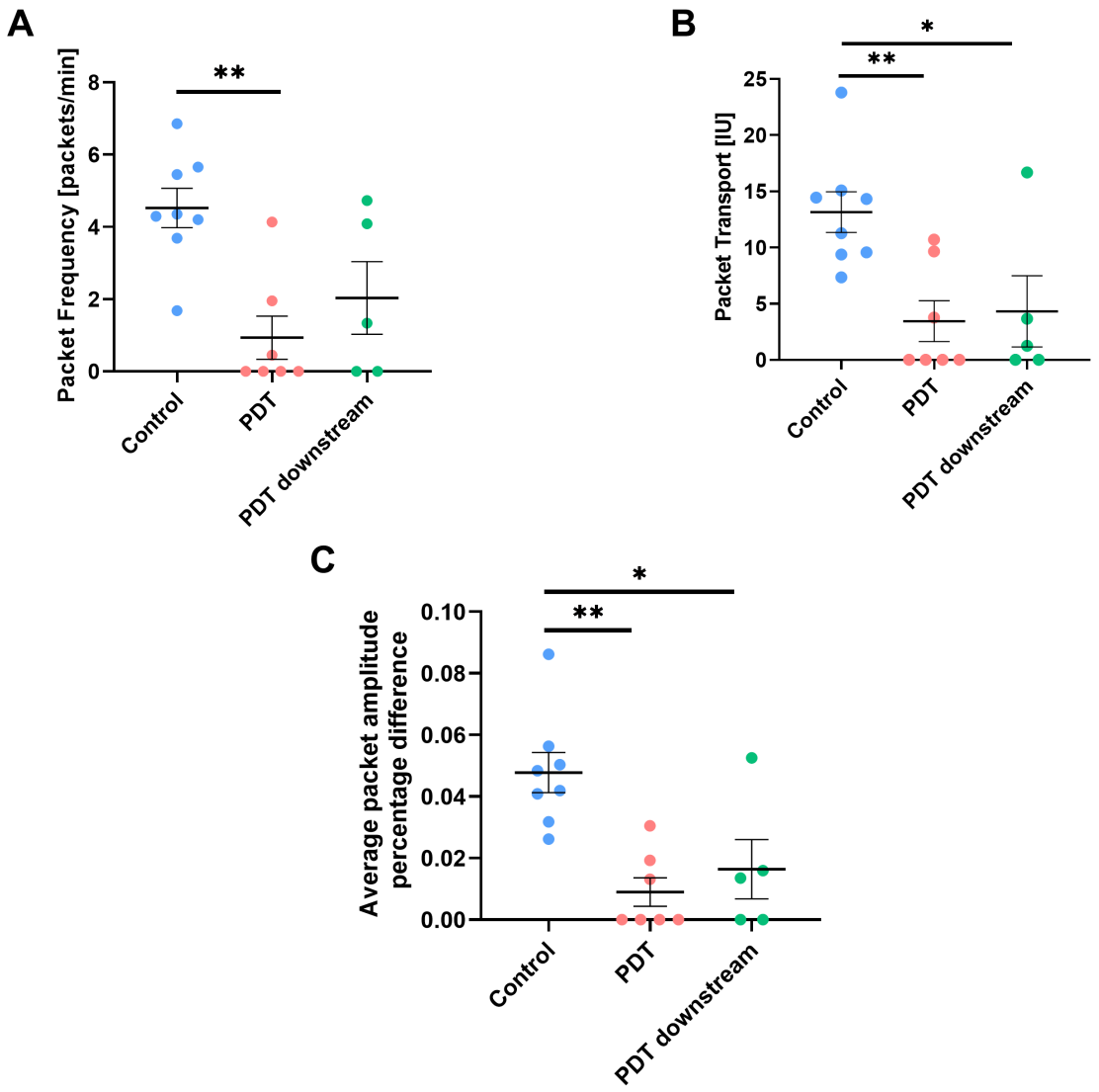

Figure 2.10: Decreased lymphatic function was observed downstream from the injury site. Function in PDT animals was evaluated at the injury site (4.5 cm from the tail tip) and proximal to it (6 cm from the tail tip). One-way ANOVA and Tuckey's multiple comparisons test *P<0.05, **P<0.01, n=8 for control group, n=7 for PDT group, n=6 for PDT downstream measurement. Error bars represent mean±SE.

2.4 Discussion

When delivered intradermally at the tip of the mouse tail, we hypothesized that verteporfin would still be taken up primarily in lymphatics, similar to other hydrophobic small molecules such as has been shown with indocyanine green, due to the rapid bind to interstitial pro-

teins and clearance by lymphatics. It has been suggested that as a protein-bound drug, verteporfin in non-liposomal formulation can be taken up by endothelial cells by binding to LDL and entering the cells through the LDL receptor [95] and given that lymphatics drain lipoproteins from the tissue space [127], such a mechanism would also be possible for lymphatics. Although complete lymphatic ablation did not occur, we observed similar results to that seen in lymphatics in the ear skin when the lower light fluence was used to activate a liposomal formulation of the drug [12]. We took advantage of this initial mild disruption in lymphatic permeability is response to PDT, to investigate the longitudinal effects of treatment and the consequence to lymphatic contractile function.

For half of the injury group, the function was restored by day 28, while the other half still did not present any pumping. Most importantly, considerable changes following the verteporfin administration and its activation were observed 72 hours after the treatment. Upstream and downstream from the treatment site, the lymphatics appeared visually normal for most of the animals, while the packet amplitude and packet transport were significantly decreased (Figure 2.9).

The most apparent change following photodynamic therapy was the change in the tail fluorescence and NIR tracer distribution. Therefore, an additional metric was introduced to estimate the fluorescent area and mean fluorescence of the tail. The mean brightness increases with the dye accumulation indicating lymphatic transport stasis. The fluorescent area represents the dye distribution within the tail. In control animals, it did not significantly change as the NIR tracer was distributed only within the collecting lymphatic vessels and limited initial lymphatics. However, in animals after the photodynamic therapy, the dye was observed to leak into the interstitium, increasing the fluorescent area of the tail occupied by tracer, and suggesting enhanced permeability due to the localized action of ROS as a result of PDT treatment. A similar pattern was presented for the normalized mean fluorescence.

Initial lymphatics were observed throughout the study in multiple animals. Therefore,

we decided to investigate if the amount of hexagonal-shaped initial lymphatics will change following the verteporfin administration and its activation. Two animals, one per each study group, were excluded as they presented a hexagonal network during the baseline measurements. As a result, the increase in the number of initial lymphatics was observed for every animal from the PDT group, starting on day 3. The number of visible initial lymphatics was decreasing, in cases where lymphatic leakage was reduced. However, those vessels remained prominent in animals with a high amount of interstitial fluid. In the control group, such a radical increase in the count of initial lymphatics was not observed. However, if they were visualized, it was at least a week after the verteporfin administration. Since initial lymphatics were taking up the NIR tracer accumulated in the interstitium following the PDT, we conclude that initial lymphatics were recruited to transport the lymph when the integrity of collecting lymphatics was compromised.

In the single vessel ligation animal model correlation between the tail swelling and lymphatic dysfunction was reported. Lymphatic dysfunction was characterized by packet transport [80]. In this study, tail swelling did not occur and the leaky lymphatics that were observed did not lead to the increased tail circumference (Figure 2.7 A). From this, we infer that the swelling is not required for the loss of lymphatic pumping function, and in PDT injury of lymphatic vessels those two results are not conjugated as in the surgical model of lymphedema.

As it was mentioned before, the packet frequency and packet transport declined following PDT (Figure 2.8, 2.9, 2.10). Simultaneously, the amount of interstitial fluid at the injury site was increased due to leakage of lymph at the site of injury. Previous studies revealed that an increased volume of dye injection leads to decreased contractility of the lymphatic vessels, even though the volumetric flow rate in the vessel is elevated [128], thus impaired contractility is not necessarily indicative of reduced lymphatic flow. On the contrary, it has been known for some time that elevated flow though lymphatic vessels can trigger a wall shear stress mediated inhibition of lymphatic contraction [129, 130, 131, 132, 133]. Based

on these reports, even though the lymphatic contractile frequency was reduced after PDT, the lack of swelling suggests that the transport of the lymph still occurs, and the leakiness is compensated for by a sufficient volume flow rate driven by interstitial fluid pressure.

In previous surgically induced injury models there was a delayed reduction in lymphatic transport in the intact vessel following the single vessel ligation model [80]. Similarly to that, the lymphatic contractile function was decreased or absent proximal to the photodynamic injury location (Figure 2.10), and loss of contraction function was delayed. Considering that inflammatory cytokines decrease collecting lymphatic pumping [134, 135], the reduced function of the lymphatics along the tail that was observed could be consequence of an inflammatory response to PDT [80].

As it has been reported before, lymphatic and blood vessels permeability can be increased as a result of photodynamic therapy [12, 95]. The efficacy of photodynamic therapy is influenced by multiple factors, such as the target area, light power, drug dosage and duration of light administration [95]. In this study, an NIR Cy5.5 filter was used for verteporfin activation, which does not target the verteporfin absorption peak that occurs between 690-695 nm (Figure 2.1). Therefore, the administered light dosage was increased by extending the exposure time. Achieved results (Figure 2.5, 2.6) are similar to the previously observed lymphatic hyperpermeability seen under low-dose liposomal verteporfin treatment [12]. One advantage to our approach was that the secondary NIR channel, in combination with injection of NIR tracers, allowed us to focus the beam directly at the depth of the collecting lymphatic vessel prior to switching over to the activation wavelength. Since the exposure area was limited through the optical set-up, this allowed up to achieve verteporfin activation exclusively in the targeted area.

Increased lymphatic permeability observed in this study correspond to the previously described effects of verteporfin. One important thing to note, is that verteporfin itself is a Yes associate protein (YAP) inhibitor [136, 137] and has been shown to suppress expression of *Ang2*, VE-cadherin, MMP2 and α-SMA [138], which facilitate angio-and lymphangio-

genesis and form the cell-cell junction between the LECs [28, 31, 139]. The YAP/TAZ pathway has also been shown to be a negative regulator of Prox1, and that inhibiting it had beneficial effects in attenuating pathological lymphangiogenesis in an inflammation model in the cornea [140]. While we cannot discount that treatment with verteporfin alone might have some baseline effect on lymphatic function and permeability, our data demonstrate that light activation is necessary to produce the observed changes, suggesting the mechanism of action is through the production of free oxygen radicals rather than through inhibition of YAP.

Photodynamic therapy could be utilized to study the effect of increased lymphatic permeability in healthy and pathophysiological states. Changes in lymphatic permeability have previously been associated with various conditions such as obesity, adipose tissue formation, and fibrosis. A suggested verteporfin application regiment provides a framework to increase lymphatic permeability and generate localized reactive oxygen species. Since the mouse tail is often used to study lymphedema, such PDT may provide an additional improvement to the single vessel ligation model as a preconditioning treatment, which may prolong the surgery effect. Additionally, such an injury would allow us to study the local impact of lymphatic leakiness on the resolution of lymphedema.

CHAPTER 3
CONCLUSION AND FUTURE WORK

The goal of this thesis was to evaluate the application of lymphatic-specific photodynamic therapy to establish an experimental model of lymphatic injury. This was accomplished in a mouse tail model through the implementation of commercially available non-liposomal verteporfin and an NIR imaging system. The same NIR setup was used to access lymphatic function with a different filter set. The mouse tail was chosen as a target location, thanks to previously established lymphedema models and provided a framework to evaluate contractile function. Additional analysis was introduced to evaluate the fluorescent area of the tail and the brightness values. For that purpose, the same images, collected as a functional measurement, were used. Considering that every single measurement out of 288 contains around 3000 images, automated processing was used. The main advantages are automated tail detection within the image, even in case of the low brightness and dye detection without overestimation, which was observed for adaptive thresholding.

As a consequence of the selected drug and light stimulation, consistent results were obtained. While the control group did not present significant changes from the baseline measurements, animals with light-activated drug showed increased permeability at the site of light exposure. Functional analysis reflected the observed changes. In the photodynamic therapy group, there were multiple days when no function was observed. In several animals, it was not restored by day 28 post-PDT, and downstream lymphatics were not visible. For this group of animals, we can conclude that partial lymphatic ablation occurred in addition to modified permeability. Therefore, the most consistent result was hyperpermeability. It was identified as NIR tracer leakage from the lymphatic vasculature into the interstitium. The maximum increase in the leakage was measured at one and two weeks following the treatment.

Based on these results, the following improvements could be implemented in future studies. The wavelength of the Cy5.5 filter was able to deliver the photodynamic therapy. In future work, the use of a light source with the wavelength matching the absorbance peak of the verteporfin at higher power density would decrease the amount of administered drug and exposure time needed, which is defined by the power density and desired energy. Such a solution could be provided, for example, by a Cy7 filter for NIR system with central wavelength 710 and FWHM 75. Further histology of tail samples will provide additional insight into biological contributions to the observed changes and the mechanism responsible for lymphatic regeneration.

This study has shown that the PDT with verteporfin can be activated in the mouse tail to alter lymphatic permeability. Another potential utilization of such findings would be a combination of PDT with a single vessel ligation model of lymphedema. Since spontaneous swelling resolution can confound results in the current animal model, preconditioning animals with the PDT before the single vessel ligation surgery may prolong the swelling and provide a framework for investigating the role of hyperpermeability in lymphatic pathology and its resolution.

Considering that reactive oxygen species are an integral part of the verteporfin activation and have a negative impact on lymphatic contractions [141], this model could be used to study oxidative stress and test the tools to suppress it. As ROS are short-lived molecules, the administration of antioxidants should be performed immediately after the PDT is conducted or as a prior treatment. Overall, the established methodology is useful in examining the ROS effect on the local tissues, lymphatic adaptation to increased permeability, and the influence of enhanced lymphatic permeability on the lymphedema progression. This framework may facilitate research focused on lymphatic regeneration, restoration of the pumping function, and mitigation of negative consequences of reactive oxygen species. The described photodynamic therapy regiment was effective *in vivo* and could be potentially applied to isolated vessels following corresponding adjustment of the administered

drug dose and exposure time.

While leaky lymphatics are observed in transgenic mouse models of lymphedema, this parameter is not extensively studied as an initial condition in various surgical models of the pathology [55, 142]. Photodynamic therapy provides a tool to induce changes without the use of transgenic animals and allows one to induce those changes locally with a high degree of regional specificity. This could create a predisposition to low-grade inflammation with dilated and leaky lymphatics [142].

In this experiment, the photodynamic therapy was a one-time procedure administered at the single site on the tail. This leads to significant changes in lymphatic contractile function both at the site of the light activation and proximal from it. Further investigation of lymphatic regeneration following such injury may involve repetitive PDT at the same location. In this case, if these procedures will be separated by sufficient time, this may prolong the obtained effect and delay lymphatic regeneration. However, it is also possible that in case of frequent administration or increased power, the procedure will lead to complete ablation of the lymphatics and lymph stasis. On the one hand, the light activation area could be expanded, and the lymphatic leakage can be induced along the whole tail to study lymphatic function and immune response to such changes in the local environment. On the other hand, reducing the treatment area to only one vessel may provide another tool to study the lymphatic adaptation and local modifications, similar to the single vessel ligation model [80] without interruption of the skin integrity.

The presented methodology describes an easily administered, non-invasive, and fast-acting procedure to induce the targeted injury of the lymphatic vessels and modify their local environment. Utilization of the existing NIR set-up allows for the continuous evaluation of the lymphatic function adaptation to the administered verteporfin-based therapy. This PDT technique may be used as an independent animal model of lymphatic hyperpermeability and ROS-affected lymphatics as well as an additional tool to improve existing animal models of lymphedema and facilitate the research toward its treatment.

Appendices

APPENDIX A

ANIMAL GROUPS

Table A.1: Animals used in the study. Rows marked in pink represent verteporfin + light group,in blue-verteporfin only group.

Animal study with 600 ug/ml Verteporfin											
Label	Gender	DOB	Age on Day 0 (Weeks)	Drug Dose	Light Dose Magnification	Day 0	Day 3	Day 7	Day 14	Day 21	Day 28
MF1	Female	12/16/2019	6	600 ug/ml	6.3	1/29/2020	2/1/2020	2/5/2020	2/12/2020	2/19/2020	2/26/2020
MF2	Female	12/16/2019	6	600 ug/ml	6.3	1/29/2020	2/1/2020	2/5/2020	2/12/2020	2/19/2020	2/26/2020
MF3	Female	12/16/2019	6	600 ug/ml	6.3	1/29/2020	2/1/2020	2/5/2020	2/12/2020	2/19/2020	2/26/2020
MF4	Female	12/16/2019	7	600 ug/ml	-	2/2/2020	2/5/2020	2/9/2020	2/16/2020	2/23/2020	3/1/2020
MF5	Female	12/16/2019	7	600 ug/ml	-	2/2/2020	2/5/2020	2/9/2020	2/16/2020	2/23/2020	3/1/2020
MF6	Female	12/30/2019	6	600 ug/ml	6.3	2/12/2020	2/15/2020	2/19/2020	2/26/2020	3/4/2020	3/11/2020
MF7	Female	12/30/2019	6	600 ug/ml	-	2/12/2020	2/15/2020	2/19/2020	2/26/2020	3/4/2020	3/11/2020
MF8	Female	12/30/2019	6	600 ug/ml	-	2/12/2020	2/15/2020	2/19/2020	2/26/2020	3/4/2020	3/11/2020
MM1	Male	12/30/2019	8	600 ug/ml	6.3	2/23/2020	2/26/2020	3/1/2020	3/8/2020	3/15/2020	3/22/2020
MM2	Male	12/30/2019	8	600 ug/ml	-	2/23/2020	2/26/2020	3/1/2020	3/8/2020	3/15/2020	3/22/2020
MM3	Male	12/30/2019	10	600 ug/ml	6.3	3/9/2020	3/12/2020	3/16/2020	3/23/2020	3/30/2020	4/6/2020
MM4	Male	12/30/2019	10	600 ug/ml	-	3/9/2020	3/12/2020	3/16/2020	3/23/2020	3/30/2020	4/6/2020
MM5	Male	12/30/2019	10	600 ug/ml	6.3	3/9/2020	3/12/2020	3/16/2020	3/23/2020	3/30/2020	4/6/2020
MM6	Male	12/30/2019	10	600 ug/ml	-	3/9/2020	3/12/2020	3/16/2020	3/23/2020	3/30/2020	4/6/2020
MM7	Male	12/30/2019	10	600 ug/ml	6.3	3/9/2020	3/12/2020	3/16/2020	3/23/2020	3/30/2020	4/6/2020
MM8	Male	12/30/2019	10	600 ug/ml	-	3/9/2020	3/12/2020	3/16/2020	3/23/2020	3/30/2020	4/6/2020

APPENDIX B

DETAILED RESULTS FOR FUNCTIONAL ANALYSIS

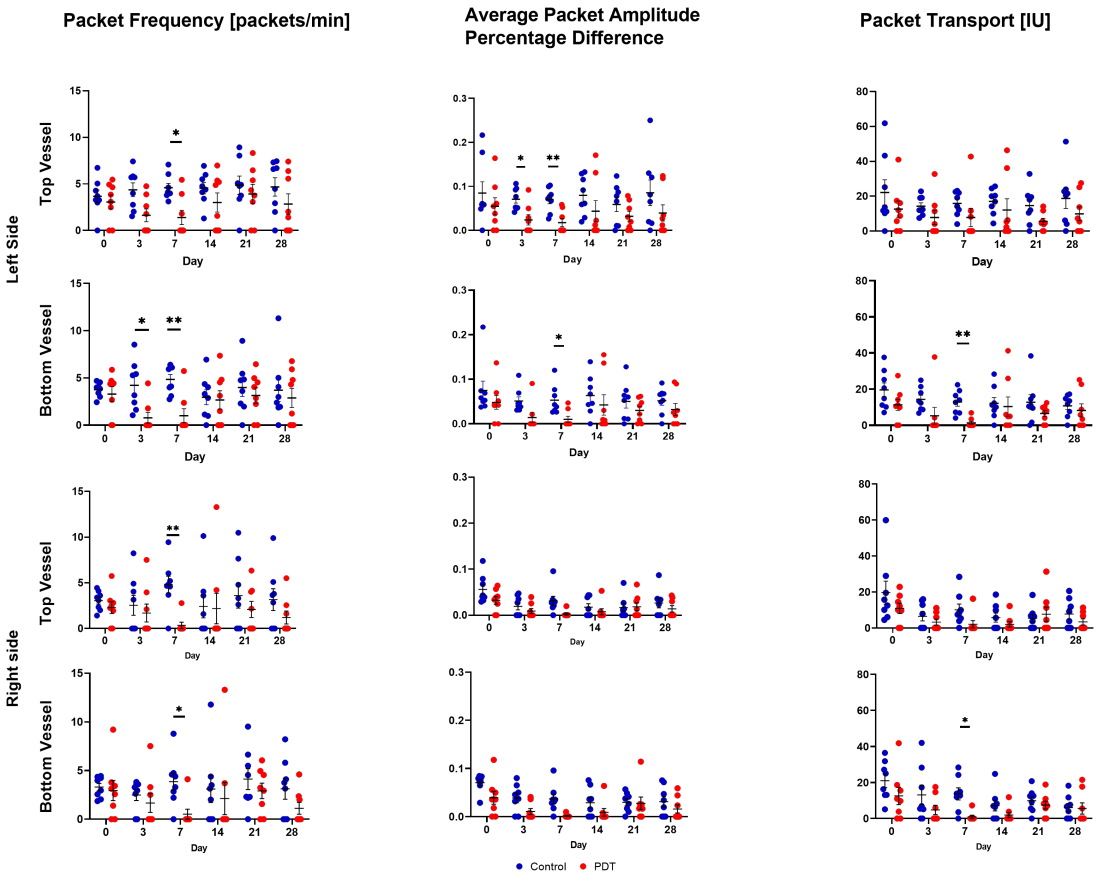

Figure B.1: Lymphatic function evaluation from left and right side of the tail at the injury site at the 4.5 cm from the tail tip.

APPENDIX C

DETAILED RESULTS FROM TAIL DETECTION ALGORITHM

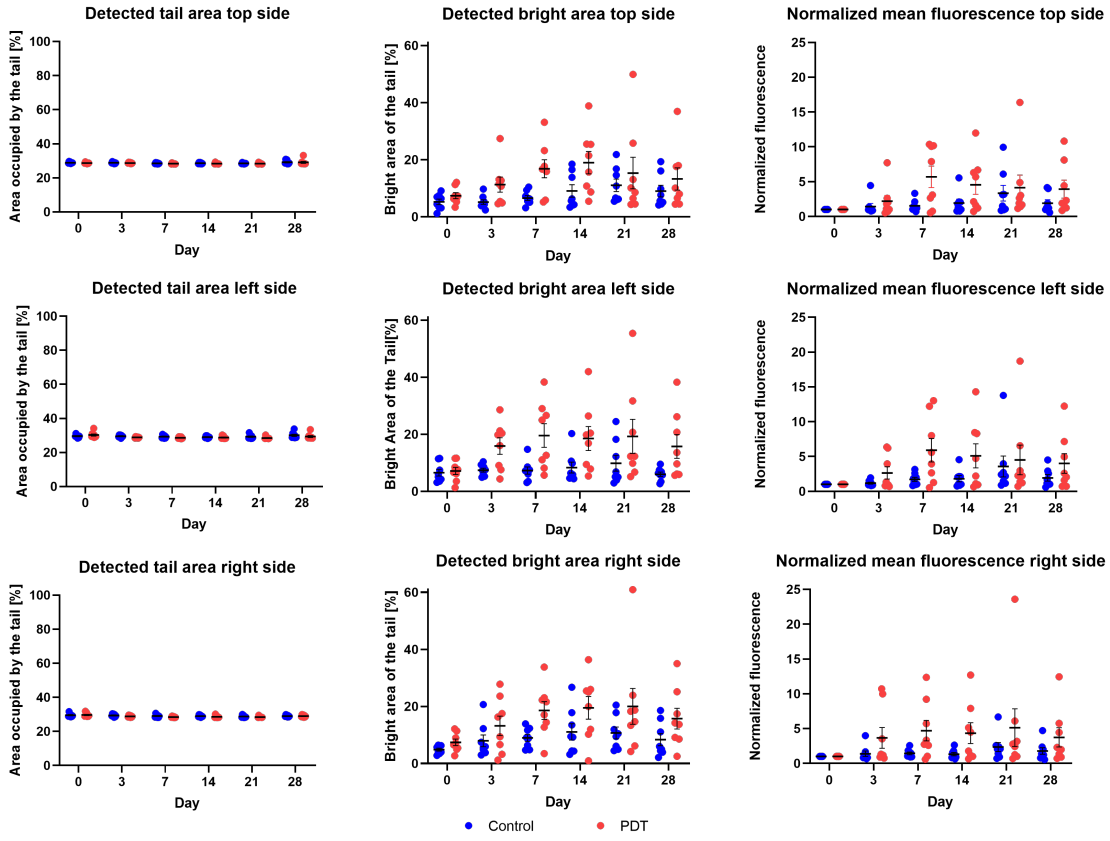

Figure C.1: Tail detection results for top, left and right sides of the tail at the 4.5 cm from the tail tip.

APPENDIX D

NORMALITY TEST OF FLUORESCENCE TAIL PERCENTAGE

Table D.1: Shapiro-Wilk normality test of fluorescence tail percentage.

Normality and Lognormality Tests of Fluorescent Tail Area %:Tabular results

	T0	C0	T3	C3	T7	C7	T14	C14	T21	C21	T28	C28
Test for normal distribution Shapiro-Wilk test												
W	0.9544	0.9471	0.9614	0.8501	0.9687	0.9199	0.9597	0.8240	0.7730	0.7649	0.8712	0.8061
P value	0.7558	0.6820	0.8234	0.0955	0.8875	0.4289	0.8076	0.0514	0.0146	0.0119	0.1548	0.0333
Passed normality test (alpha=0.05)?	Yes	Yes	Yes	Yes	Yes	Yes	Yes	Yes	No	No	Yes	No
P value summary	ns	ns	ns	ns	ns	ns	ns	ns	*	*	ns	*
Number of values	8	8	8	8	8	8	8	8	8	8	8	8

APPENDIX E

NORMALITY TEST OF MEAN TAIL FLUORESCENCE

Table E.1: Shapiro-Wilk normality test of mean tail fluorescence normalized to the baseline measurement. T stands for PDT group, C-control group, following number represents the day of the measurement.

Normality and Lognormality Tests of MeanFluorescence:Tabular results

	T0	C0	T3	C3	T7	C7	T14	C14	T21	C21	T28	C28
Test for normal distribution												
Shapiro-Wilk test												
W	Invalid input data	Invalid input data	0.7466	0.6110	0.9115	0.8971	0.8724	0.7751	0.6213	0.7349	0.8097	0.8682
P value			0.0075	0.0002	0.3651	0.2719	0.1590	0.0154	0.0003	0.0056	0.0363	0.1449
Passed normality test (alpha=0.05)?			No	No	Yes	Yes	Yes	No	No	No	No	Yes
P value summary			**	***	ns	ns	ns	*	***	**	*	ns
Number of values	8	8	8	8	8	8	8	8	8	8	8	8

APPENDIX F

NORMALITY TEST OF PACKET FREQUENCY

Table F.1: Shapiro-Wilk normality test of packet frequency normalized to the baseline measurement. T stands for PDT group, C-control group, following number represents the day of the measurement.

Normality and Lognormality Tests of NormalPacketFrequency_revised:Tabular results

	T0	C0	T3	C3	T7	C7	T14	C14	T21	C21	T28	C28
Test for normal distribution												
Shapiro-Wilk test												
W	Invalid input data	Invalid input data	0.6793	0.9603	0.6412	0.9746	0.7672	0.9859	0.8890	0.9882	0.8531	0.9877
P value			0.0022	0.8133	0.0008	0.9316	0.0191	0.9860	0.2694	0.9917	0.1311	0.9907
Passed normality test (alpha=0.05)?			No	Yes	No	Yes	No	Yes	Yes	Yes	Yes	Yes
P value summary			**	ns	***	ns	*	ns	ns	ns	ns	ns
Number of values	7	8	7	8	7	8	7	8	7	8	7	8

APPENDIX G

NORMALITY TEST OF PACKET TRANSPORT

Table G.1: Shapiro-Wilk normality test of packet transport normalized to the baseline measurement. T stands for PDT group, C-control group, following number represents the day of the measurement.

Normality and Lognormality Tests of NormPacketTransport_revised:Tabular results

	T0	C0	T3	C3	T7	C7	T14	C14	T21	C21	T28	C28
Test for normal distribution												
Shapiro-Wilk test												
W	Invalid input data	Invalid input data	0.7637	0.5403	0.7384	0.6602	0.8404	0.9040	0.7920	0.7805	0.8044	0.8683
P value			0.0176	<0.0001	0.0096	0.0008	0.1001	0.3135	0.0341	0.0177	0.0453	0.1449
Passed normality test (alpha=0.05)?			No	No	No	No	Yes	Yes	No	No	No	Yes
P value summary			*	****	**	***	ns	ns	*	*	*	ns
Number of values	7	8	7	8	7	8	7	8	7	8	7	8

APPENDIX H

NORMALITY TEST OF PACKET AMPLITUDE

Table H.1: Shapiro-Wilk normality test of packet amplitude percentage difference normalized to the baseline measurement. T stands for PDT group, C-control group, following number represents the day of the measurement.

Normality and Lognormality Tests of PacketAmplitued_revised:Tabular results

	T0	C0	T3	C3	T7	C7	T14	C14	T21	C21	T28	C28
Test for normal distribution												
Shapiro-Wilk test												
W	Invalid input data	Invalid input data	0.7528	0.7293	0.6824	0.8071	0.6555	0.9026	0.8306	0.8478	0.7819	0.8969
P value			0.0136	0.0048	0.0024	0.0341	0.0012	0.3048	0.0811	0.0906	0.0270	0.2712
Passed normality test (alpha=0.05)?			No	No	No	No	No	Yes	Yes	Yes	No	Yes
P value summary			*	**	**	*	**	ns	ns	ns	*	ns
Number of values	7	8	7	8	7	8	7	8	7	8	7	8

APPENDIX I

IMAGE PROCESSING CODE

```
# Tail Detection Code
import os
import glob
import imageio
import numpy as np
from scipy import stats
import matplotlib.pyplot as plt

class mice_experiment:


    def __init__(self):
        self.processing_option = 1
        self.input_dir = os.getcwd()
        self.output_dir = os.getcwd()


    def prepare_stats_container(self):
        stats = dict()
        stats['tail_area'] = []
        stats['bright_area'] = []
        stats['max_value'] = []
        stats['min_value'] = []
        stats['mean_value'] = []
        stats['median_value'] = []
        return stats

    ################################################
    # Checking the folder and based on that        #
    # generates output folder                      #
    ################################################
    def init_output_structure(self,folder):
        if os.path.exists(folder):
            print(f'Generating output directory {folder}_output')
            self.input_dir = os.path.join(os.getcwd(),folder)
            self.output_dir = os.path.join(os.getcwd(),folder + '_output
                ')

            if not os.path.exists(self.output_dir):
                os.mkdir(self.output_dir)
            return True

        else:
            print('This folder does not exist, try another one ;)')
            return False

    ########################################
    ########################################
    def perform_analysis(self):

        # Initial check of the files in the main folder
        stats = self.prepare_stats_container()
        stats = self.go_through_files(self.input_dir, self.output_dir,
            stats)
```

```
53          self.output_stats(self.output_dir, stats)
54
55          # retrieving all the files from the folder and all its
                subfolders
56          for root, dirs, files in os.walk(self.input_dir):
57              for folder in dirs:
58                  input_dir = os.path.join(root,folder)
59
60                  # created to output folder
61      output_dir = os.path.join(self.output_dir,root[len(self.input_dir)
            +1:],folder)
62                  stats = self.prepare_stats_container()
63                  if not os.path.exists(output_dir):
64                      os.mkdir(output_dir)
65
66                  # performs analysis for the folder
67                  stats = self.go_through_files(input_dir,output_dir,
                        stats)
68
69                  # generates the files with the results
70                  self.output_stats(output_dir, stats)
71
72      def go_through_files(self, input_dir, output_dir, stats):
73          files_to_process = glob.glob(input_dir + '\*.tif', recursive=
                True)
74          print(f'Processing: {input_dir}')
75          count = 0
76          for path in files_to_process:
77              try:
78                  data = imageio.imread(path).astype('uint16')
79              except (ValueError,PermissionError):
80                  print(f'non accessible file. Skipping {path}')
81                  continue
82
83              stats, whole_tail, local_image  = self.process_image(data,
                    stats)
84              count = count + 1
85              if count % 500 == 0:
86                  count = 0
87      imageio.imwrite(os.path.join(output_dir,path[path.rfind('\\')+1:-4]+
            '.png'),whole_tail)
88      imageio.imwrite(os.path.join(output_dir,path[path.rfind('\\')+1:-4]+
            '_bright.png'),local_image)
89
90          return stats
91
92      def normalize_data(self, data):
93          return ((data - np.min(data)) / (np.max(data) - np.min(data)))
                *255
94
95      ################################################
96      # Image processing                             #
97      ################################################
98      def process_image(self, image, stats):
```

```
        # normalizeing the image
        local_image = np.copy(image/256)
        local_image = self.normalize_data(local_image)
        local_image = (local_image).astype(np.uint8)

        threshold = np.quantile(local_image,0.72)
        whole_tail = np.copy(local_image)
        whole_tail[whole_tail < threshold] = 0

        stats['tail_area'].append(np.count_nonzero(whole_tail > 0))
        stats['max_value'].append(np.max(image[whole_tail > 0]))
        stats['min_value'].append(np.min(image[whole_tail > 0]))
        stats['median_value'].append(np.median(image[whole_tail > 0]))
        stats['mean_value'].append(np.mean(image[whole_tail > 0]))


        # extracting the brightest spots
        if self.processing_option == 1:
            threshold = np.quantile(local_image,0.90)
            local_image[local_image < threshold] = 0

            for i in range(0,512):
                column = local_image[:,i]
                threshold = np.quantile(column,0.93)
                column[column < threshold] = 0
                local_image[:,i]=column

        else:
            mean_value = np.mean(whole_tail[whole_tail > 0])
            percentage = 0.8
            threshold = np.max(local_image[whole_tail > 0]) -
             (np.max(local_image[whole_tail > 0])
              - mean_value) * percentage
            #print(mean_value,threshold,np.max(local_image[whole_tail >
               0]))
            local_image[local_image < threshold] = 0
        stats['bright_area'].append(np.count_nonzero(local_image > 0))
        return stats, whole_tail, local_image

    def output_stats(self, output_dir, stats):
        if len(stats['tail_area']) > 0:

        plt.figure()
        plt.plot(stats['tail_area'], marker='o', drawstyle="steps-post")
        ax = plt.gca()
        ax.ticklabel_format(useOffset=False)
        plt.savefig(os.path.join(output_dir,'tail_area.png'))
        plt.close()

        plt.figure()
        plt.plot(stats['mean_value'], marker='o', drawstyle="steps-post"
           )
        ax = plt.gca()
        ax.ticklabel_format(useOffset=False)
```

```
        plt.savefig(os.path.join(output_dir,'mean_value.png'))
        plt.close()

        plt.figure()
        plt.plot(np.array(stats['tail_area'])/(512*512), marker='o',
            drawstyle="steps-post")
        ax = plt.gca()
        ax.ticklabel_format(useOffset=False)
        plt.savefig(os.path.join(output_dir,'tail_area_percentage.png'))
        plt.close()

        plt.figure()
        plt.plot(stats['bright_area'], marker='o', drawstyle="steps-post
            ")
        ax = plt.gca()
        ax.ticklabel_format(useOffset=False)
        plt.savefig(os.path.join(output_dir,'m_bright_area.png'))
        plt.close()

        plt.figure()
        plt.plot(stats['max_value'], marker='o', drawstyle="steps-post")
        ax = plt.gca()
        ax.ticklabel_format(useOffset=False)
        plt.savefig(os.path.join(output_dir,'max_value.png'))
        plt.close()

        plt.figure()
        plt.plot(stats['min_value'], marker='o', drawstyle="steps-post")
        ax = plt.gca()
        ax.ticklabel_format(useOffset=False)
        plt.savefig(os.path.join(output_dir,'min_value.png'))
        plt.close()

        plt.figure()
        plt.plot(stats['median_value'], marker='o', drawstyle="steps-
            post")
        ax = plt.gca()
        ax.ticklabel_format(useOffset=False)
        plt.savefig(os.path.join(output_dir,'median_value.png'))
        plt.close()

        plt.figure()
        plt.plot(np.array(stats['bright_area'])/np.array(stats['
            tail_area']),
        marker='o', drawstyle="steps-post")
        ax = plt.gca()
        ax.ticklabel_format(useOffset=False)
            plt.savefig(os.path.join(output_dir,'percentage.png'))
        plt.close()


        with open(os.path.join(output_dir,'data.csv'),'w') as f:
            f.write('tail area,bright area,max value,min value,median
                value,mean value\n')
```

```
            for i in range(0,len(stats['bright_area'])):
                f.write("%.1f,%.1f,%.1f,%.1f,%.1f,%.1f\n" %
                (stats['tail_area'][i],stats['bright_area'][i],stats['
                    max_value'][i]\
                ,stats['min_value'][i],stats['median_value'][i],stats['
                    mean_value'][i]))


def main():

    extract = mice_experiment()
    found_folder = False

    while not found_folder:
        folder_name = input('Folder to be analyzed: ')
        found_folder = extract.init_output_structure(folder_name)

    which_filter = input('Do you want to use mean filtering? [y/n]')

    if which_filter == 'y' or which_filter == 'Y':
        extract.processing_option = 2

    # start going through files
    extract.perform_analysis()

if __name__ == "__main__":
    main()
```

APPENDIX J
DATA PROCESSING CODE

```
import os
import glob
import pandas as pd
import numpy as np
from scipy import stats

class csv_analysis:

    def search_for_folder(self,folder):
        if os.path.exists(folder):
            self.name = folder[folder.rfind(os.path.sep)+1:folder.rfind(
                '_')]
            print(f'Found directory {folder},\nGenenerating output file
                {self.name}.csv')
            self.input_dir = os.path.join(os.getcwd(),folder)
            return True

        else:
            print('This directory does not exist)')
            return False

    def prepare_container(self, keys):
        stats = dict()
        stats['folder name'] = []
        for key in keys:
            stats[key] = []
            stats[key + " error"] = []
            stats[key + " var"] = []
            stats[key + " std"] = []


        return stats

    def generate_folder_name(self,csv_file):
        name = csv_file.lower()

        if name.find('pos0') != -1:
            name = name[0:name.find('pos0')-1]
            return name[name.rfind(os.path.sep)+1:].upper()

        name = name[0:name.rfind(os.path.sep)-1]
        return name[name.rfind(os.path.sep)+1:].upper()

    def search_csv(self):
        files_to_process = glob.glob(self.input_dir + os.path.sep +'**'+
            os.path.sep + '*.csv', recursive=True)
        if len(files_to_process):
            # read the first found csv to gather the keys used
            data = pd.read_csv(files_to_process[0])
            output_container = self.prepare_container(data.keys())

            for csv_file in files_to_process:
                data = pd.read_csv(csv_file)
                if 'folder name' in data.keys():
```

```
                    continue

                for key in data.keys():
                    output_container[key].append(np.mean(data[key]))
                    output_container[key + " error"].append(stats.sem(
                        data[key]))
                    output_container[key + " var"].append(np.var(data[
                        key]))
                    output_container[key + " std"].append(np.std(data[
                        key]))
                output_container['folder name'].append(self.
                    generate_folder_name(csv_file))
                data = None

            self.output_to_file( output_container)

    def output_to_file(self,stats):
        data = pd.DataFrame.from_dict(stats)
        data.to_csv(os.path.join(self.input_dir, self.name + '.csv'),
            index=False)

def main():
    extract = csv_analysis()
    found_folder = False

    while not found_folder:
        folder_name = input('Folder to be analyzed: ')
        found_folder = extract.search_for_folder(folder_name)
    extract.search_csv()

if __name__ == "__main__":
    main()
```

REFERENCES

[1] J. B. Dixon, "Lymphatic lipid transport: sewer or subway?", *Trends in Endocrinology & Metabolism*, vol. 21, no. 8, pp. 480–487, 2010.

[2] J. W. Breslin, Y. Yang, J. P. Scallan, R. S. Sweat, S. P. Adderley, and W. L. Murfee, "Lymphatic vessel network structure and physiology", *Comprehensive Physiology*, vol. 9, no. 1, pp. 207–299, 2019.

[3] G. J. Randolph, V. Angeli, and M. A. Swartz, "Dendritic-cell trafficking to lymph nodes through lymphatic vessels", *Nature Reviews Immunology*, vol. 5, no. 8, pp. 617–628, 2005.

[4] M. A. Swartz, "The physiology of the lymphatic system", *Advanced Drug Delivery Reviews*, vol. 50, no. 1-2, pp. 3–20, 2001. arXiv: 1003.3921v1.

[5] E. M. Renkin, "Some consequences of capillary permeability to macromolecules: Starling's hypothesis reconsidered", *American Journal of Physiology-Heart and Circulatory Physiology*, vol. 250, no. 5, H706–H710, 1986.

[6] R Gerli, R Solito, E Weber, and M Aglianó, "Specific adhesion molecules bind anchoring filaments and endothelial cells in human skin initial lymphatics.", *Lymphology*, vol. 33, no. 4, pp. 148–157, 2000.

[7] H. Wiig, D. Keskin, and R. Kalluri, "Interaction between the extracellular matrix and lymphatics: consequences for lymphangiogenesis and lymphatic function", *Matrix biology : journal of the International Society for Matrix Biology*, vol. 29, no. 8, pp. 645–656, 2010.

[8] L. V. Leak and J. F. Burke, "Ultrastructural studies on the lymphatic anchoring filaments", *The Journal of cell biology*, vol. 36, no. 1, pp. 129–149, 1968.

[9] M. Furman and F. Gallo, *The Neurophysics of Human Behavior Explorations at the Interface of Brain, Mind, Behavior, and Information*. 2000, ISBN: 9781420040432.

[10] G. Sacchi, E. Weber, M. Agliano, N. Raffaelli, and L. Comparini, "The structure of superficial lymphatics in the human thigh: precollectors", *The Anatomical Record*, vol. 247, no. 1, pp. 53–62, 1997.

[11] E. Bazigou, J. T. Wilson, and J. E. Moore, "Primary and secondary lymphatic valve development: Molecular, functional and mechanical insights", *Microvascular Research*, vol. 96, pp. 38–45, 2014.

[12] W. W. Kilarski, A. Muchowicz, M. Wachowska, R. Mężyk-Kopeć, J. Golab, M. A. Swartz, and P. Nowak-Sliwinska, "Optimization and regeneration kinetics of lymphatic-specific photodynamic therapy in the mouse dermis", *Angiogenesis*, vol. 17, no. 2, pp. 347–357, 2014.

[13] J. P. Scallan, S. D. Zawieja, J. A. Castorena-Gonzalez, and M. J. Davis, "Lymphatic pumping: mechanics, mechanisms and malfunction", *The Journal of Physiology*, vol. 594, no. 20, pp. 5749–5768, 2016.

[14] K. K. M. Murphy, *Janeway's immunobiology*, Ninth edition.. 2017, ISBN: 9780815345053.

[15] A. N. Kogan and U. H. von Andrian, "Lymphocyte Trafficking", in *Microcirculation*, Elsevier, 2008, pp. 449–482, ISBN: 9780123745309.

[16] T. H. Adair and A. C. Guyton, "Modification of lymph by lymph nodes. III. Effect of increased lymph hydrostatic pressure", *American Journal of Physiology - Heart and Circulatory Physiology*, vol. 18, no. 4, 1985.

[17] J. Banchereau and R. M. Steinman, "Dendritic cells and the control of immunity", *Nature*, vol. 392, no. 6673, pp. 245–252, 1998.

[18] K. Nakamura and S. G. Rockson, "The role of the lymphatic circulation in the natural history and expression of cardiovascular disease", *International Journal of Cardiology*, vol. 129, no. 3, pp. 309–317, 2008.

[19] W. L. Olszewski and A. Engeset, "Intrinsic contractility of prenodal lymph vessels and lymph flow in human leg", *American Journal of Physiology-Heart and Circulatory Physiology*, vol. 239, no. 6, H775–H783, 1980.

[20] C. M. Quick, A. M. Venugopal, A. A. Gashev, D. C. Zawieja, and R. H. Stewart, "Intrinsic pump-conduit behavior of lymphangions", *American Journal of Physiology-Regulatory, Integrative and Comparative Physiology*, vol. 292, no. 4, R1510–R1518, 2007.

[21] L. Causey, S. C. Cowin, and S. Weinbaum, "Quantitative model for predicting lymph formation and muscle compressibility in skeletal muscle during contraction and stretch", *Proceedings of the National Academy of Sciences of the United States of America*, vol. 109, no. 23, pp. 9185–9190, 2012.

[22] D. C. Zawieja, "Contractile physiology of lymphatics", *Lymphatic Research and Biology*, vol. 7, no. 2, pp. 87–96, 2009.

[23] K. Akagi, Y. Ikeda, M. Miyazaki, T. Abe, J. Kinoshita, Y. Maehara, and K. Sugimachi, "Vascular endothelial growth factor-C (VEGF-C) expression in human col-

orectal cancer tissues", *British Journal of Cancer*, vol. 83, no. 7, pp. 887–891, 2000.

[24] M. S. Pepper and M. Skobe, "Lymphatic endothelium", *Journal of Cell Biology*, vol. 163, no. 2, pp. 209–213, 2003.

[25] S. Breiteneder-Geleff, A. Soleiman, H. Kowalski, R. Horvat, G. Amann, E. Kriehuber, K. Diem, W. Weninger, E. Tschachler, K. Alitalo, and D. Kerjaschki, "Angiosarcomas express mixed endothelial phenotypes of blood and lymphatic capillaries: Podoplanin as a specific marker for lymphatic endothelium", *American Journal of Pathology*, vol. 154, no. 2, pp. 385–394, 1999.

[26] S Banerji, J Ni, S Wang, S Clasper, J Su, R Tammi, M Jones, and D. Jackson, "LYVE-1, a new homologue of the CD44 glycoprotein", *Journal of Cell Biology*, vol. 144, no. 4, pp. 789–801, 1999.

[27] N. L. Harvey, R. S. Srinivasan, M. E. Dillard, N. C. Johnson, M. H. Witte, K. Boyd, M. W. Sleeman, and G. Oliver, "Lymphatic vascular defects promoted by Prox1 haploinsufficiency cause adult-onset obesity", *Nature Genetics*, vol. 37, no. 10, pp. 1072–1081, 2005.

[28] P. Baluk, J. Fuxe, H. Hashizume, T. Romano, E. Lashnits, S. Butz, D. Vestweber, M. Corada, C. Molendini, E. Dejana, and D. M. McDonald, "Functionally specialized junctions between endothelial cells of lymphatic vessels", *Journal of Experimental Medicine*, vol. 204, no. 10, pp. 2349–2362, 2007.

[29] F. Zhang, G. Zarkada, J. Han, J. Li, A. Dubrac, R. Ola, G. Genet, K. Boyé, P. Michon, S. E. Künzel, J. P. Camporez, A. K. Singh, G. H. Fong, M. Simons, P. Tso, C. Fernández-Hernando, G. I. Shulman, W. C. Sessa, and A. Eichmann, "Lacteal junction zippering protects against diet-induced obesity", *Science*, vol. 361, no. 6402, pp. 599–603, 2018.

[30] D. O. Miteva, J. M. Rutkowski, J. B. Dixon, W. Kilarski, J. D. Shields, and M. A. Swartz, "Transmural Flow Modulates Cell and Fluid Transport Functions of Lymphatic Endothelium", *Circulation Research*, vol. 106, no. 5, pp. 920–931, 2010.

[31] W. Zheng, H. Nurmi, S. Appak, A. Sabine, E. Bovay, E. A. Korhonen, F. Orsenigo, M. Lohela, G. D'Amico, T. Holopainen, C. C. Leow, E. Dejana, T. V. Petrova, H. G. Augustin, and K. Alitalo, "Angiopoietin 2 regulates the transformation and integrity of lymphatic endothelial cell junctions", *Genes and Development*, vol. 28, no. 14, pp. 1592–1603, 2014.

[32] M. Sawane, K. Kajiya, H. Kidoya, M. Takagi, F. Muramatsu, and N. Takakura, "Apelin Inhibits Diet-Induced Obesity by Enhancing Lymphatic and Blood Vessel Integrity", *Diabetes*, vol. 62, no. 6, pp. 1970–1980, 2013.

[33] C. H. Sloop, L. Dory, and S Paul, “Interstitial fluid lipoproteins”, vol. 28, pp. 225–237, 1987.

[34] J. P. Scallan and V. H. Huxley, “In vivo determination of collecting lymphatic vessel permeability to albumin : a role for lymphatics in exchange”, *The Journal of physiology,*, vol. 588, pp. 243–254, 2010.

[35] T. P. Padera, A. Kadambi, E. Di Tomaso, C. Mouta Carreira, E. B. Brown, Y. Boucher, N. C. Choi, D. Mathisen, J. Wain, E. J. Mark, L. L. Munn, and R. K. Jain, “Lymphatic metastasis in the absence of functional intratumor lymphatics”, *Science*, vol. 296, no. 5574, pp. 1883–1886, 2002.

[36] N. Isaka, T. P. Padera, J. Hagendoorn, D. Fukumura, and R. K. Jain, “Peritumor Lymphatics Induced by Vascular Endothelial Growth Factor-C Exhibit Abnormal Function”, *Cancer Research*, vol. 64, no. 13, pp. 4400–4404, 2004.

[37] M. Skobe, L. M. Hamberg, T. Hawighorst, M. Schirner, G. L. Wolf, K. Alitalo, and M. Detmar, “Concurrent induction of lymphangiogenesis, angiogenesis, and macrophage recruitment by vascular endothelial growth factor-C in melanoma”, *American Journal of Pathology*, vol. 159, no. 3, pp. 893–903, 2001.

[38] S. Hirakawa, L. F. Brown, S. Kodama, K. Paavonen, K. Alitalo, and M. Detmar, “VEGF-C-induced lymphangiogenesis in sentinel lymph nodes promotes tumor metastasis to distant sites”, *Blood*, vol. 109, no. 3, pp. 1010–1017, 2007.

[39] J. P. Scallan, M. A. Hill, and M. J. Davis, “Lymphatic vascular integrity is disrupted in type 2 diabetes due to impaired nitric oxide signalling”, *Cardiovascular research*, vol. 107, pp. 89–97, 2015.

[40] N. L. Harvey, “The Link between Lymphatic Function and Adipose Biology”, *Annals of the New York Academy of Sciences*, vol. 1131, no. 1, pp. 82–88, 2008.

[41] “Collecting Lymphatic Vessel Permeability Facilitates Adipose Tissue Inflammation and Distribution of Antigen to Lymph Node–Homing Adipose Tissue Dendritic Cells”, *The Journal of Immunology*, vol. 194, no. 11, pp. 5200–5210, 2015.

[42] H Brorson, H Svensson, K Norrgren, and O Thorsson, “Liposuction reduces arm lymphedema without significantly altering the already impaired lymph transport.”, *Lymphology*, vol. 31, no. 4, pp. 156–172, 1998.

[43] T. Avraham, J. C. Zampell, A. Yan, S. Elhadad, E. S. Weitman, S. G. Rockson, J. Bromberg, and B. J. Mehrara, “Th2 differentiation is necessary for soft tissue fibrosis and lymphatic dysfunction resulting from lymphedema”, *FASEB journal : official publication of the Federation of American Societies for Experimental Biology*, vol. 27, no. 3, pp. 1114–1126, 2013.

[44] R. Tabibiazar, L. Cheung, J. Han, J. Swanson, A. Beilhack, A. An, S. S. Dadras, N. Rockson, S. Joshi, R. Wagner, and S. G. Rockson, "Inflammatory Manifestations of Experimental Lymphatic Insufficiency", *PLoS medicine*, vol. 3, no. 7, 2006.

[45] "Regulation of adipogenesis by lymphatic fluid stasis: part I. Adipogenesis, fibrosis, and inflammation", *Plastic and reconstructive surgery*, vol. 129, no. 4, pp. 825–834, 2012.

[46] J. C. Zampell, A. Yan, S. Elhadad, T. Avraham, E. Weitman, and B. J. Mehrara, "CD4+ Cells Regulate Fibrosis and Lymphangiogenesis in Response to Lymphatic Fluid Stasis", *PLOS ONE*, vol. 7, no. 11, e49940, 2012.

[47] P. D. McMaster and S. Hudack, "II. INDUCED ALTERATIONS IN THE PERMEABILITY OF THE LYMPHATIC CAPILLARY", *The Journal of Experimental Medicine*, vol. 56, no. 2, pp. 239–253, 1932.

[48] W. E. Cromer, S. D. Zawieja, B. Tharakan, E. W. Childs, M. K. Newell, and D. C. Zawieja, "The effects of inflammatory cytokines on lymphatic endothelial barrier function", *Angiogenesis*, vol. 17, no. 2, pp. 395–406, 2014. arXiv: NIHMS150003.

[49] Y. Kakei, M. Akashi, T. Shigeta, T. Hasegawa, and T. Komori, "Alteration of Cell–Cell Junctions in Cultured Human Lymphatic Endothelial Cells with Inflammatory Cytokine Stimulation", *Lymphatic Research and Biology*, vol. 12, no. 3, pp. 136–143, 2014.

[50] S. Schwager and M. Detmar, "Inflammation and lymphatic function", *Frontiers in Immunology*, vol. 10, no. February, pp. 1–11, 2019.

[51] S. Karaman, M. Hollmén, S. Y. Yoon, H. F. Alkan, K. Alitalo, C. Wolfrum, and M. Detmar, "Transgenic overexpression of VEGF-C induces weight gain and insulin resistance in mice", *Scientific Reports*, vol. 6, pp. 1–12, 2016.

[52] K. Kajiya, S. Hirakawa, and M. Detmar, "Vascular endothelial growth factor-A mediates ultraviolet B-induced impairment of lymphatic vessel function", *American Journal of Pathology*, vol. 169, no. 4, pp. 1496–1503, 2006.

[53] S. G. Rockson, "Lymphedema", *The American Journal of Medicine*, vol. 110, no. 4, pp. 288–295, 2001.

[54] J. E. Moore and C. D. Bertram, "Lymphatic System Flows", *Annual Review of Fluid Mechanics*, vol. 50, no. 1, pp. 459–482, 2018.

[55] S. H. Azhar, H. Y. Lim, B.-K. Tan, and V. Angeli, "The Unresolved Pathophysiology of Lymphedema", *Frontiers in Physiology*, vol. 11, no. March, pp. 1–11, 2020.

[56] T. V. Petrova, T. Karpanen, C. Norrmén, R. Mellor, T. Tamakoshi, D. Finegold, R. Ferrell, D. Kerjaschki, P. Mortimer, S. Ylä-Herttuala, N. Miura, and K. Alitalo, "Defective valves and abnormal mural cell recruitment underlie lymphatic vascular failure in lymphedema distichiasis", *Nature Medicine*, vol. 10, no. 9, pp. 974–981, 2004.

[57] H. F. Falls and E. D. Kertesz, "A NEW SYNDROME COMBINING PTERYGIUM COLLI WITH DEVELOPMENTAL ANOMALIES OF THE EYELIDS AND LYMPHATICS OF THE LOWER EXTREMITIES.", *Transactions of the American Ophthalmological Society*, vol. 62, pp. 248–75, 1964.

[58] R. E. Ferrell, K. L. Levinson, J. H. Esman, M. A. Kimak, E. C. Lawrence, M. M. Barmada, and D. N. Finegold, "Hereditary lymphedema : evidence for linkage and genetic heterogeneity", *Human Molecular Genetics*, vol. 7, no. 13, pp. 2073–2078, 1998.

[59] G. Brice and S. W. Thames, "Milroy disease and the VEGFR-3 mutation phenotype", *Journal of medical genetics*, vol. 42, no. 2, pp. 98–102, 2005.

[60] G. Kristiana, S. Dörte, B. Glen, S. M. A., R. M. Guy, v. I. Andreas, C. Fiona, K. Kamini, J. Steve, M. P. S., M. Sahar, S.-M. Stefan, and O. Pia, "Mutation in Vascular Endothelial Growth Factor-C, a Ligand for Vascular Endothelial Growth Factor Receptor-3, Is Associated With Autosomal Dominant Milroy-Like Primary Lymphedema", *Circulation Research*, vol. 112, no. 6, pp. 956–960, 2013.

[61] M. J. Taylor, A. Hoerauf, and M. Bockarie, "Lymphatic filariasis and onchocerciasis", *The Lancet*, vol. 376, no. 9747, pp. 1175–1185, 2010.

[62] K. M. Pfarr, A. Y. Debrah, S. Specht, and A. Hoerauf, "Filariasis and lymphoedema", *Parasite Immunology*, vol. 31, no. 11, pp. 664–672, 2009.

[63] L. E. Warren, C. L. Miller, N. Horick, M. N. Skolny, L. S. Jammallo, B. T. Sadek, M. N. Shenouda, J. A. O'Toole, S. M. MacDonald, M. C. Specht, and A. G. Taghian, "The Impact of Radiation Therapy on the Risk of Lymphedema After Treatment for Breast Cancer: A Prospective Cohort Study", *International Journal of Radiation Oncology*Biology*Physics*, vol. 88, no. 3, pp. 565–571, 2014.

[64] C. Shah and F. A. Vicini, "Breast Cancer-Related Arm Lymphedema: Incidence Rates, Diagnostic Techniques, Optimal Management and Risk Reduction Strategies", *International Journal of Radiation Oncology*Biology*Physics*, vol. 81, no. 4, pp. 907–914, 2011.

[65] H Wiig, K Rubin, and R. K. Reed, "New and active role of the interstitium in control of interstitial fluid pressure: potential therapeutic consequences", *Acta Anaesthesiologica Scandinavica*, vol. 47, no. 2, pp. 111–121, 2003.

[66] W. L. Olszewski, "Contractility Patterns of Normal and Pathologically Changed Human Lymphatics", *Annals of the New York Academy of Sciences*, vol. 979, no. 1, pp. 52–63, 2002.

[67] M. Mihara, H. Hara, Y. Hayashi, M. Narushima, T. Yamamoto, T. Todokoro, T. Iida, N. Sawamoto, J. Araki, K. Kikuchi, N. Murai, T. Okitsu, I. Kisu, and I. Koshima, "Pathological Steps of Cancer-Related Lymphedema: Histological Changes in the Collecting Lymphatic Vessels after Lymphadenectomy", *PLoS ONE*, vol. 7, no. 7, A. Greene, Ed., e41126, 2012.

[68] F. Ogata, K. Fujiu, I. Koshima, R. Nagai, and I. Manabe, "Phenotypic modulation of smooth muscle cells in lymphoedema", *British Journal of Dermatology*, vol. 172, no. 5, pp. 1286–1293, 2015.

[69] S. Babu, S. Q. Bhat, N. Pavan Kumar, A. B. Lipira, S. Kumar, C. Karthik, V. Kumaraswami, and T. B. Nutman, "Filarial Lymphedema Is Characterized by Antigen-Specific Th1 and Th17 Proinflammatory Responses and a Lack of Regulatory T Cells", *PLoS Neglected Tropical Diseases*, vol. 3, no. 4, R. T. Fujiwara, Ed., e420, 2009.

[70] R. Anuradha, P. J. George, L. E. Hanna, V. Chandrasekaran, P. Kumaran, T. B. Nutman, and S. Babu, "IL-4–, TGF-β–, and IL-1–Dependent Expansion of Parasite Antigen-Specific Th9 Cells Is Associated with Clinical Pathology in Human Lymphatic Filariasis", *The Journal of Immunology*, vol. 191, no. 5, pp. 2466–2473, 2013. arXiv: NIHMS150003.

[71] G. D. García Nores, C. L. Ly, I. L. Savetsky, R. P. Kataru, S. Ghanta, G. E. Hespe, S. G. Rockson, and B. J. Mehrara, "Regulatory T Cells Mediate Local Immunosuppression in Lymphedema", *Journal of Investigative Dermatology*, vol. 138, no. 2, pp. 325–335, 2018.

[72] S. Ghanta, D. A. Cuzzone, J. S. Torrisi, N. J. Albano, W. J. Joseph, I. L. Savetsky, J. C. Gardenier, D. Chang, J. C. Zampell, and B. J. Mehrara, "Regulation of inflammation and fibrosis by macrophages in lymphedema", *American Journal of Physiology - Heart and Circulatory Physiology*, vol. 308, no. 9, H1065–H1077, 2015.

[73] L. Andersen, I. Højris, M. Erlandsen, and J. Andersen, "Treatment of Breast-Cancer-related Lymphedema With or Without Manual Lymphatic Drainage: A Randomized Study", *Acta Oncologica*, vol. 39, no. 3, pp. 399–405, 2000.

[74] C. M. Badger, J. L. Peacock, and P. S. Mortimer, "A randomized, controlled, parallel-group clinical trial comparing multilayer bandaging followed by hosiery versus hosiery alone in the treatment of patients with lymphedema of the limb.", *Cancer*, vol. 88, no. 12, pp. 2832–7, 2000.

[75] R. Koul, T. Dufan, C. Russell, W. Guenther, Z. Nugent, X. Sun, and A. L. Cooke, "Efficacy of complete decongestive therapy and manual lymphatic drainage on treatment-related lymphedema in breast cancer", *International Journal of Radiation Oncology*Biology*Physics*, vol. 67, no. 3, pp. 841–846, 2007.

[76] J. C. Gardenier, G. E. Hespe, R. P. Kataru, I. L. Savetsky, J. S. Torrisi, G. D. G. Nores, J. J. Dayan, D. Chang, J. Zampell, I. Martínez-Corral, S. Ortega, and B. J. Mehrara, "Diphtheria toxin–mediated ablation of lymphatic endothelial cells results in progressive lymphedema", *JCI Insight*, vol. 1, no. 15, pp. 1–15, 2016.

[77] T. Mäkinen, L. Jussila, T. Veikkola, T. Karpanen, M. I. Kettunen, K. J. Pulkkanen, R. Kauppinen, D. G. Jackson, H. Kubo, S.-I. Nishikawa, S. Ylä-Herttuala, and K. Alitalo, "Inhibition of lymphangiogenesis with resulting lymphedema in transgenic mice expressing soluble VEGF receptor-3", *Nature Medicine*, vol. 7, no. 2, pp. 199–205, 2001.

[78] R. S. Srinivasan, M. E. Dillard, O. V. Lagutin, F.-J. Lin, S. Tsai, M.-J. Tsai, I. M. Samokhvalov, and G. Oliver, "Lineage tracing demonstrates the venous origin of the mammalian lymphatic vasculature", *Genes & Development*, vol. 21, no. 19, pp. 2422–2432, 2007.

[79] M. T. Dellinger, R. J. Hunter, M. J. Bernas, M. H. Witte, and R. P. Erickson, "Chy - 3 mice are Vegfc haploinsufficient and exhibit defective dermal superficial to deep lymphatic transition and dermal lymphatic hypoplasia", *Developmental Dynamics*, vol. 236, no. 8, pp. 2346–2355, 2007.

[80] M. J. Weiler, M. T. Cribb, Z. Nepiyushchikh, T. S. Nelson, and J. B. Dixon, "A novel mouse tail lymphedema model for observing lymphatic pump failure during lymphedema development", *Scientific Reports*, no. October 2016, pp. 1–15, 2019.

[81] Y. Kawashima, M. Sugimura, Y.-C. Hwang, and N. Kudo, "The lymph system in mice", *Japanese Journal of Veterinary Research*, vol. 12, no. 4, pp. 69–78, 1964.

[82] J. M. Rutkowski, M. Moya, J. Johannes, J. Goldman, and M. A. Swartz, "Secondary lymphedema in the mouse tail: Lymphatic hyperplasia, VEGF-C upregulation, and the protective role of MMP-9", *Microvascular Research*, vol. 72, no. 3, pp. 161–171, 2006.

[83] M. A. Swartz, A. Kaipainen, P. A. Netti, C. Brekken, Y. Boucher, A. J. Grodzinsky, and R. K. Jain, "Mechanics of interstitial-lymphatic fluid transport: theoretical foundation and experimental validation", *Journal of Biomechanics*, vol. 32, no. 12, pp. 1297–1307, 1999.

[84] U. Mendez, E. M. Stroup, L. L. Lynch, A. B. Waller, and J. Goldman, "A chronic and latent lymphatic insufficiency follows recovery from acute lymphedema in the

rat foreleg", *American Journal of Physiology-Heart and Circulatory Physiology*, vol. 303, no. 9, H1107–H1113, 2012.

[85] D. Tobbia, J. Semple, A. Baker, D. Dumont, A. Semple, and M. Johnston, "Lymphedema Development and Lymphatic Function following Lymph Node Excision in Sheep", *Journal of Vascular Research*, vol. 46, no. 5, pp. 426–434, 2009.

[86] A. Szuba, M. Skobe, M. J. Karkkainen, W. S. Shin, D. P. Beynet, N. B. Rockson, N. Dakhil, S. Spilman, M. L. Goris, H. W. Strauss, T. Quertermous, K. Alitalo, and S. G. Rockson, "Therapeutic lymphangiogenesis with human recombinant VEGF-C", *The FASEB Journal*, vol. 16, no. 14, pp. 1985–1987, 2002.

[87] F. S. Frueh, E. Gousopoulos, F. Rezaeian, M. D. Menger, N. Lindenblatt, and P. Giovanoli, "Animal models in surgical lymphedema research–a systematic review.", *The Journal of surgical research*, vol. 200, no. 1, pp. 208–220, 2016.

[88] R. A. Mittra and L. J. Singerman, "Recent Advances in the Management of Age-Related Macular Degeneration", *Optometry and Vision Science*, vol. 79, no. 4, 2002.

[89] T. J. Dougherty, C. J. Gomer, B. W. Henderson, G. Jori, D. Kessel, M. Korbelik, J. Moan, and Q. Peng, "Photodynamic Therapy", *JNCI Journal of the National Cancer Institute*, vol. 90, no. 12, pp. 889–905, 1998.

[90] J. A. Leman and C. A. Morton, "Photodynamic therapy: applications in dermatology", *Expert Opinion on Biological Therapy*, vol. 2, no. 1, pp. 45–53, 2002.

[91] D. E. Dolmans, D. Fukumura, and R. K. Jain, "Photodynamic therapy for cancer", *Nature Reviews Cancer*, vol. 3, no. 5, pp. 380–387, 2003.

[92] H. Abrahamse and M. R. Hamblin, "New photosensitizers for photodynamic therapy", *Biochemical Journal*, vol. 473, no. 4, pp. 347–364, 2016.

[93] "VISUDYNE [package insert], Bausch & Lomb Incorporated", 2000.

[94] A. Fahr, P. V. Hoogevest, S. May, N. Bergstrand, and M. L. S. Leigh, "Transfer of lipophilic drugs between liposomal membranes and biological interfaces: Consequences for drug delivery", *European Journal of Pharmaceutical Sciences*, vol. 26, no. 3-4, pp. 251–265, 2005.

[95] U. Schmidt-Erfurth and T. Hasan, "Mechanisms of Action of Photodynamic Therapy with Verteporfin for the Treatment of Age-Related Macular Degeneration", *Survey of Ophthalmology*, vol. 45, no. 3, pp. 195–214, 2000.

[96] A. Ormond and H. Freeman, "Dye Sensitizers for Photodynamic Therapy", *Materials*, vol. 6, no. 3, pp. 817–840, 2013.

[97] L. Kong, Y. Zhao, L. Dong, Y. Jian, X. Jin, B. Li, Y. Feng, M. Liu, X. Liu, and H. Wu, "Non-contact detection of oxygen saturation based on visible light imaging device using ambient light", *Optics Express*, vol. 21, no. 15, p. 17 464, 2013.

[98] L. Amselem, J. M. Monés, and L. Arias, "Photosensitizers and photodynamic therapyverteporfin", in *Retinal Pharmacotherapy*, Ldl, vol. 55, Elsevier, 2010, pp. 297–305.

[99] M. Clement, G. Daniel, and M. Trelles, "Optimising the design of a broad-band light source for the treatment of skin", *Journal of Cosmetic and Laser Therapy*, vol. 7, no. 3-4, pp. 177–189, 2005.

[100] M. Wachowska, A. Osiak, A. Muchowicz, M. Gabrysiak, A. Domagała, W. W. Kilarski, and J. Golab, "Investigation of cell death mechanisms in human lymphatic endothelial cells undergoing photodynamic therapy", *Photodiagnosis and Photodynamic Therapy*, vol. 14, pp. 57–65, 2016.

[101] R Aquaron, O Forzano, J. L. Murati, G Fayet, C Aquaron, and B Ridings, "Simple, reliable and fast spectrofluorometric method for determination of plasma Verteporfin (Visudyne) levels during photodynamic therapy for choroidal neovascularization.", *Cellular and molecular biology (Noisy-le-Grand, France)*, vol. 48, no. 8, pp. 925–930, 2002.

[102] A. Milasan, F. Dallaire, G. Mayer, and C. Martel, "Effects of LDL Receptor Modulation on Lymphatic Function", *Scientific Reports*, vol. 6, no. 1, p. 27 862, 2016.

[103] T. Tammela, A. Saaristo, T. Holopainen, S. Ylä-Herttuala, L. C. Andersson, S. Virolainen, I. Immonen, and K. Alitalo, "Photodynamic ablation of lymphatic vessels and intralymphatic cancer cells prevents metastasis", *Science Translational Medicine*, vol. 3, no. 69, pp. 1–8, 2011.

[104] W. W. Kilarski, "Physiological Perspective on Therapies of Lymphatic Vessels", *Advances in Wound Care*, vol. 7, no. 7, pp. 189–208, 2018.

[105] A. Muchowicz, M. Wachowska, J. Stachura, K. Tonecka, M. Gabrysiak, D. Wołosz, Z. Pilch, W. W. Kilarski, L. Boon, T. J. Klaus, and J. Golab, "Inhibition of lymphangiogenesis impairs antitumour effects of photodynamic therapy and checkpoint inhibitors in mice", *European Journal of Cancer*, vol. 83, pp. 19–27, 2017.

[106] J. C. Rasmussen, I. C. Tan, M. V. Marshall, C. E. Fife, and E. M. Sevick-Muraca, "Lymphatic imaging in humans with near-infrared fluorescence", *Current Opinion in Biotechnology*, vol. 20, no. 1, pp. 74–82, 2009.

[107] S. Yousefi, Zhongwei Zhi, and R. K. Wang, "Label-Free Optical Imaging of Lymphatic Vessels Within Tissue Beds IN VIVO", *IEEE Journal of Selected Topics in Quantum Electronics*, vol. 20, no. 2, pp. 15–24, 2014.

[108] "MRI of the Central Lymphatic System", *Topics in Magnetic Resonance Imaging*, vol. 26, no. 4, pp. 175–180, 2017.

[109] "Role of contrast enhanced MRI lymphangiography in evaluation of lower extremity lymphatic vessels for patients with primary lymphedema", *Egyptian Journal of Radiology and Nuclear Medicine*, vol. 49, no. 3, pp. 776–781, 2018.

[110] J. Rao, A. Dragulescu-Andrasi, and H. Yao, "Fluorescence imaging in vivo: recent advances", *Current Opinion in Biotechnology*, vol. 18, no. 1, pp. 17–25, 2007.

[111] M. Weiler, T. Kassis, and J. B. Dixon, "Sensitivity analysis of near-infrared functional lymphatic imaging", *Journal of Biomedical Optics*, vol. 17, no. 6, p. 066 019, 2012.

[112] T. Kitai, T. Inomoto, M. Miwa, and T. Shikayama, "Fluorescence navigation with indocyanine green for detecting sentinel lymph nodes in breast cancer", *Breast Cancer*, vol. 12, no. 3, pp. 211–215, 2005.

[113] M. Fujiwara, T. Mizukami, A. Suzuki, and H. Fukamizu, "Sentinel lymph node detection in skin cancer patients using real-time fluorescence navigation with indocyanine green: preliminary experience", *Journal of Plastic, Reconstructive & Aesthetic Surgery*, vol. 62, no. 10, e373–e378, 2009.

[114] N. Tagaya, R. Yamazaki, A. Nakagawa, A. Abe, K. Hamada, K. Kubota, and T. Oyama, "Intraoperative identification of sentinel lymph nodes by near-infrared fluorescence imaging in patients with breast cancer", *The American Journal of Surgery*, vol. 195, no. 6, pp. 850–853, 2008.

[115] E. M. Sevick-Muraca, R. Sharma, J. C. Rasmussen, M. V. Marshall, J. A. Wendt, H. Q. Pham, E. Bonefas, J. P. Houston, L. Sampath, K. E. Adams, D. K. Blanchard, R. E. Fisher, S. B. Chiang, R. Elledge, and M. E. Mawad, "Imaging of lymph flow in breast cancer patients after microdose administration of a near-infrared fluorophore: Feasibility study", *Radiology*, vol. 246, no. 3, pp. 734–741, 2008.

[116] Y. Ogasawara, H. Ikeda, M. Takahashi, K. Kawasaki, and H. Doihara, "Evaluation of Breast Lymphatic Pathways with Indocyanine Green Fluorescence Imaging in Patients with Breast Cancer", *World Journal of Surgery*, vol. 32, no. 9, pp. 1924–1929, 2008.

[117] N. Unno, M. Nishiyama, M. Suzuki, N. Yamamoto, K. Inuzuka, D. Sagara, H. Tanaka, and H. Konno, "Quantitative Lymph Imaging for Assessment of Lymph

Function using Indocyanine Green Fluorescence Lymphography", *European Journal of Vascular and Endovascular Surgery*, vol. 36, no. 2, pp. 230–236, 2008.

[118] M. Weiler and J. B. Dixon, "Differential transport function of lymphatic vessels in the rat tail model and the long-term effects of Indocyanine Green as assessed with near-infrared imaging", *Frontiers in Physiology*, vol. 4, no. August, pp. 1–10, 2013.

[119] S. T. Proulx, P. Luciani, A. Christiansen, S. Karaman, K. S. Blum, M. Rinderknecht, J.-C. Leroux, and M. Detmar, "Use of a PEG-conjugated bright near-infrared dye for functional imaging of rerouting of tumor lymphatic drainage after sentinel lymph node metastasis", *Biomaterials*, vol. 34, no. 21, pp. 5128–5137, 2013.

[120] T. S. Nelson, R. E. Akin, M. J. Weiler, T. Kassis, J. A. Kornuta, and J. B. Dixon, "Minimally invasive method for determining the effective lymphatic pumping pressure in rats using near-infrared imaging", *American Journal of Physiology-Regulatory, Integrative and Comparative Physiology*, vol. 306, no. 5, R281–R290, 2014.

[121] A. A. Gashev, T. Nagai, and E. A. Bridenbaugh, "Indocyanine Green and Lymphatic Imaging: Current Problems", *Lymphatic Research and Biology*, vol. 8, no. 2, pp. 127–130, 2010.

[122] J. C. Kraft and R. J. Y. Ho, "Interactions of Indocyanine Green and Lipid in Enhancing Near-Infrared Fluorescence Properties: The Basis for Near-Infrared Imaging in Vivo", *Biochemistry*, vol. 53, no. 8, pp. 1275–1283, 2014.

[123] Novartis Ophthalmics, *Visudyne (verteporfin for injection). Professional Product Labeling. NDA 21-119/S-001.* 2001.

[124] "Endothelin-1 inhibits size dependent lymphatic clearance of PEG-based conjugates after intra-articular injection into the rat knee", *Acta Biomaterialia*, vol. 93, pp. 270–281, 2019.

[125] C. Chong, F. Scholkmann, S. B. Bachmann, P. Luciani, J.-C. Leroux, M. Detmar, and S. T. Proulx, "In vivo visualization and quantification of collecting lymphatic vessel contractility using near-infrared imaging", *Scientific Reports*, vol. 6, no. 1, p. 22 930, 2016.

[126] T. S. Nelson, "The functional and remodeling response of collecting lymphatic vessels to disruption of lymphatic drainage pathways", PhD thesis, Georgia Institute of Technology, 2018.

[127] H. Y. Lim, C. H. Thiam, K. P. Yeo, R. Bisoendial, C. S. Hii, K. C. McGrath, K. W. Tan, A. Heather, J. S. J. Alexander, and V. Angeli, "Lymphatic Vessels Are Essential for the Removal of Cholesterol from Peripheral Tissues by SR-BI-Mediated Transport of HDL", *Cell Metabolism*, vol. 17, no. 5, pp. 671–684, 2013.

[128] E. M. Bouta, C. Blatter, T. A. Ruggieri, E. F. Meijer, L. L. Munn, B. J. Vakoc, and T. P. Padera, "Lymphatic function measurements influenced by contrast agent volume and body position", *JCI Insight*, vol. 3, no. 2, 2018.

[129] A. A. Gashev, "Inhibition of the active lymph pump by flow in rat mesenteric lymphatics and thoracic duct", *The Journal of Physiology*, vol. 540, no. 3, pp. 1023–1037, 2002.

[130] A. A. GASHEV, "Physiologic aspects of lymphatic contractile function", *Annals of the New York Academy of Sciences*, vol. 979, no. 1, pp. 178–187,

[131] A. Koller, R. Mizuno, and G. Kaley, "Flow reduces the amplitude and increases the frequency of lymphatic vasomotion: Role of endothelial prostanoids", *American Journal of Physiology - Regulatory Integrative and Comparative Physiology*, vol. 277, no. 6 46-6, pp. 1683–1689, 1999.

[132] J. A. Kornuta, Z. Nepiyushchikh, O. Y. Gasheva, A. Mukherjee, D. C. Zawieja, and J. B. Dixon, "Effects of dynamic shear and transmural pressure on wall shear stress sensitivity in collecting lymphatic vessels", *American Journal of Physiology - Regulatory Integrative and Comparative Physiology*, vol. 309, no. 9, R1122–R1134, 2015.

[133] A. Mukherjee, J. Hooks, Z. Nepiyushchikh, and J. B. Dixon, "Entrainment of Lymphatic Contraction to Oscillatory Flow", *Scientific Reports*, vol. 9, no. 1, pp. 1–14, 2019.

[134] S. D. Zawieja, W. Wang, X. Wu, Z. V. Nepiyushchikh, D. C. Zawieja, and M. Muthuchamy, "Impairments in the intrinsic contractility of mesenteric collecting lymphatics in a rat model of metabolic syndrome", *American Journal of Physiology-Heart and Circulatory Physiology*, vol. 302, no. 3, H643–H653, 2012.

[135] S. Liao, G. Cheng, D. A. Conner, Y. Huang, R. S. Kucherlapati, L. L. Munn, N. H. Ruddle, R. K. Jain, D. Fukumura, and T. P. Padera, "Impaired lymphatic contraction associated with immunosuppression", *Proceedings of the National Academy of Sciences*, vol. 113, no. 40, E5992–E5992, 2016.

[136] Y. Liu-Chittenden, B. Huang, J. S. Shim, Q. Chen, S.-J. Lee, R. A. Anders, J. O. Liu, and D. Pan, "Genetic and pharmacological disruption of the TEAD-YAP complex suppresses the oncogenic activity of YAP", *Genes & Development*, vol. 26, no. 12, pp. 1300–1305, 2012.

[137] K. Brodowska, A. Al-Moujahed, A. Marmalidou, M. Meyer zu Horste, J. Cichy, J. W. Miller, E. Gragoudas, and D. G. Vavvas, "The clinically used photosensitizer Verteporfin (VP) inhibits YAP-TEAD and human retinoblastoma cell growth in

vitro without light activation", *Experimental Eye Research*, vol. 124, pp. 67–73, 2014.

[138] H. Wei, F. Wang, Y. Wang, T. Li, P. Xiu, J. Zhong, X. Sun, and J. Li, "Verteporfin suppresses cell survival, angiogenesis and vasculogenic mimicry of pancreatic ductal adenocarcinoma via disrupting the YAP-TEAD complex", *Cancer Science*, vol. 108, no. 3, pp. 478–487, 2017.

[139] H. T. Du, L. L. Du, X. L. Tang, H. Y. Ge, and P. Liu, "Blockade of MMP-2 and MMP-9 inhibits corneal lymphangiogenesis", *Graefe's Archive for Clinical and Experimental Ophthalmology*, vol. 255, no. 8, pp. 1573–1579, 2017.

[140] H. Cho, J. Kim, J. H. Ahn, Y.-K. Hong, T. Mäkinen, D.-S. Lim, and G. Y. Koh, "YAP and TAZ Negatively Regulate Prox1 During Developmental and Pathologic Lymphangiogenesis", *Circulation Research*, vol. 124, no. 2, pp. 225–242, 2018.

[141] D. C. Zawieja, S. T. Greiner, K. L. Davis, W. M. Hinds, and H. J. Granger, "Reactive oxygen metabolites inhibit spontaneous lymphatic contractions", *American Journal of Physiology - Heart and Circulatory Physiology*, vol. 260, no. 6 29-6, 1991.

[142] G. E. Hespe, C. L. Ly, R. P. Kataru, and B. J. Mehrara, "Baseline Lymphatic Dysfunction Amplifies the Negative Effects of Lymphatic Injury", *Plastic and Reconstructive Surgery*, vol. 143, no. 1, 77e–87e, 2019.